

The diverse broad-band lightcurves of Swift GRBs reproduced with the cannonball model

Shlomo Dado¹, Arnon Dar², A. De Rújula³

ABSTRACT

Two radiation mechanisms, inverse Compton scattering (ICS) and synchrotron radiation (SR), suffice within the cannonball (CB) model of long gamma ray bursts (LGRBs) and X-ray flashes (XRFs) to provide a very simple and accurate description of their observed prompt emission and afterglows. Simple as they are, the two mechanisms and the burst environment generate the rich structure of the light curves at all frequencies and times. This is demonstrated for 33 selected Swift LGRBs and XRFs, which are well sampled from early until late time and faithfully represent the entire diversity of the broad-band light curves of Swift LGRBs and XRFs. Their prompt gamma-ray and X-ray emission is dominated by ICS of ‘glory’ light. During their fast decline phase, ICS is taken over by SR, which dominates their broad-band afterglow. The pulse shape and spectral evolution of the gamma-ray peaks and the early-time X-ray flares, and even the delayed optical ‘humps’ in XRFs, are correctly predicted. The ‘canonical’ and non-canonical X-ray light curves and the chromatic behaviour of the broad-band afterglows are well reproduced. In particular, in canonical X-ray light curves, the initial fast decline and rapid softening of the prompt emission, the transition to the plateau phase, the subsequent gradual steepening of the plateau to an asymptotic power-law decay, and the transition from chromatic to achromatic behaviour of the light curves agrees well with those predicted by the CB model. The Swift early-time data on XRF 060218 are inconsistent with a black-body emission from a shock break-out through a stellar envelope. Instead, they are well described by ICS of glory light by a jet breaking out from SN2006aj.

Subject headings: gamma rays: bursts

¹dado@phep3.technion.ac.il, Physics Department, Technion, Haifa 32000, Israel

² arnon@physics.technion.ac.il, Physics Department, Technion, Haifa 32000, Israel
dar@cern.ch, Theory Unit, CERN, 1211 Geneva 23, Switzerland

³alvaro.derujula@cern.ch; Theory Unit, CERN, 1211 Geneva 23, Switzerland
Physics Department, Boston University, USA

1. Introduction

Since the launch of the Swift satellite, precise data from its Burst Alert Telescope (BAT) and X-Ray Telescope (XRT) have been obtained on the spectral and temporal behaviour of the X-ray emission of long-duration γ -ray bursts (LGRBs) and X-ray flashes (XRFs) from their beginning until late times. The early data are often complemented by the ultraviolet-optical telescope (UVOT) on board Swift, and by ground-based *UVO* and *NIR* robotic and conventional telescopes. The ensemble of these data have already been used to test the most-studied theories of long duration GRBs and their afterglows (AGs), the *Fireball* (FB) models (see, e.g. Zhang & Mészáros 2004, Zhang 2007, and references therein) and the *Cannonball* (CB) model [see, e.g. Dar & De Rújula 2004 (hereafter DD2004), Dado, Dar & De Rújula (hereafter DDD) 2002a, 2003a, and references therein].

The Swift X-ray light curves of LGRBs roughly divide into two classes, ‘canonical’ and non-canonical (Nousek et al. 2006, O’Brien et al. 2006, Zhang 2007). When measured early enough, the observed X-ray emission has prompt peaks which coincide with the γ -ray peaks of the GRB, and a rapidly declining light curve with a fast spectral softening after the last detectable peak of the GRB. This rapid decline and spectral softening of the prompt emission end within a few hundreds of seconds. In canonical LGRBs the X-ray light curve turns sharply into a much flatter ‘plateau’ with a much harder power-law spectrum, typically lasting thousands to tens of thousands of seconds, and within a time of order one day it steepens into a power-law decay, which lasts until the X-ray AG becomes too dim to be detected (Fig. 1).

The plateau phase is missing in non canonical GRBs, and the asymptotic power-law decline begins the decay of the prompt emission and lasts until the X-ray become too dim to be detected (Fig. 2) without any observable break.

In an significant fraction of otherwise canonical GRBs, the rapid decay and fast spectral softening of the prompt emission changes to a slower power-law decay, $\sim t^{-2.1}$, and a harder spectrum, before it reaches the plateau (Fig. 3). We shall refer to such light curves as ‘semi-canonical’.

The Swift X-ray data show a flaring activity in a large fraction of GRBs, both at early and late times. The X-ray peaks during the prompt γ -ray emission follow the pattern of the γ -ray pulses, they must have a common origin. In many GRBs, superimposed on the early-time fast decaying X-ray light curve, there are X-ray flares, whose peak intensities also decrease with time and whose accompanying γ -ray emission is probably below the detection sensitivity of BAT. Yet, their spectral and temporal behaviour is similar to that of the prompt X/ γ pulses. Very often the flaring activity continues into the afterglow phase. Late-time

flares appear to exhibit different temporal and spectral behaviours than early-time flares.

Neither the general trend, nor the frequently complex structure of the Swift X-ray data were predicted by (or can be easily accommodated within) the standard FB models (see, e.g. Zhang & Mészáros 2004, Piran 2005, for reviews). Much earlier confrontations between predictions of the FB models and the observations also provided severe contradictions, such as the failure to understand the prompt spectrum on grounds of synchrotron radiation (e.g. Ghisellini, Celotti, & Lazzati 2000), or the ‘energy crisis’ in the comparison of the bolometric prompt and AG fluences (e.g. Piran 1999, 2000). We have discussed elsewhere other problems of FB models (DD2004, Dar 2005 and references therein), including those related to ‘jet breaks’ (e.g. DDD2002a, Dar 2005, DDD2006), and the a-posteriori explanations of the reported detections (GRB 021206: Coburn and Boggs 2003, see however Wigger et al. 2004 and Rutledge & Fox 2004; GRBs 930131 and GRB 960924: Willis et al. 2005; GRB 041219A: Kalemci et al. 2007; McGlynn et al. 2007) of large γ -ray polarization (DDD2007b, and references therein).

The Swift data have challenged the prevailing views on GRBs. Kumar et al. (2007) concluded that the prompt γ -ray emission cannot be produced in shocks, internal or external. Zhang, Liang & Zhang (2007) found that the fast decay and rapid spectral softening ending the prompt emission cannot be explained by high latitude emission. The X-ray and optical afterglows of Swift GRBs are very chromatic at early time in contrast with the fireball model expectation. Moreover, Curran et al. (2006) have carefully examined Swift data and found that X-ray and optical AGs have chromatic breaks which differ significantly from the jet break of the blast-wave model of AGs. Burrows and Racusin (2007) examined the XRT light curves of the first ~ 150 Swift GRBs and reported that the expected jet breaks are extremely rare. In particular, Liang et al. (2008) have analyzed the Swift X-ray data for the 179 GRBs detected between January 2005 and January 2007 and the optical AGs of 57 pre- and post-Swift GRBs. They did not find any burst satisfying all the criteria of a jet break.

In spite of the above failures, not all authors are so critical. Some posit that the Swift data require only some modifications of the standard FB models to accommodate the results (e.g. Panaitescu et al. 2006, Dai et al. 2007, Sato et al. 2007). Others still view the situation with faith (e.g. Covino et al. 2006, Panaitescu 2008, Dai et al. 2008, Racusin et al. 2008a).

The situation concerning the CB model is different. The model was based on the assumption that LGRBs are produced by highly relativistic jets of plasmoids of ordinary matter (Shaviv & Dar 1995) ejected in core-collapse supernova (SN) explosions akin to SN1998bw (Dar & Plaga 1999, Dar & De Rújula 2000). It successfully described the broad-band AGs observed before the Swift era (e.g. DDD2002a, DDD2003a) and exposed the consistent photometric evidence for a LGRB/SN association in all nearby GRBs (DDD2002a, DD2004 and

references therein) long before GRB 030329. In the case of GRB 030329 the first ~ 6 days of AG data were described by the CB model precisely enough to extrapolate them to predict even the date in which its associated SN would be bright enough to be detected spectroscopically (DDD2003c). General acceptance of the GRB-SN association waited until the spectroscopic discovery of SN2003dh, coincident with GRB 030329 (Hjorth et al. 2003, Stanek et al. 2003), and other spectroscopically-proven associations, e.g. GRB030213/SN2003lw (Malesani et al. 2004), GRB021211/SN2002lt (Della Valle et al. 2003), XRF060218/SN2006aj (Campana et al. 2006b, Pian et al. 2006, Mazzali et al. 2006) and XRF080109/SN2008D (Malesani et al. 2008, Modjaz et al. 2008, Soderberg et al. 2008).

The CB model (DD2004) has been applied successfully to explain all the main observed properties of long GRBs and XRFs before the Swift era (e.g. Dar 2005 and references therein). The model is summarized in §2. For detailed accounts see, e.g., De Rújula, 2007a,b.

In this report we extend and refine our analysis of the temporal and spectral behaviour of the γ -ray, X-ray and optical light curves of GRBs during the prompt emission, the rapid-decay phase, and the afterglow phase. The observed prompt spectrum in the γ -ray to X-ray domain is the predicted one, which is Compton-dominated in the CB model (DD2004). The observed widths of the γ -ray and X-ray peaks, as well as lag-times between them and their relative fluences, are in accordance with the model’s predictions, if free-free absorption dominates the transparency of the CBs to eV photons in the CBs’ rest frame. We investigate whether or not the CB model can describe all the data in terms of only two emission mechanisms: inverse Compton scattering and synchrotron radiation. We shall see that this simple picture, explicitly based on the predictions in DDD2002a and DD2004, gives a straightforward and successful description of the Swift GRB data, at all observed energies and times.

An exploding SN illuminates the progenitor’s earlier ejecta, creating a *glory* of scattered and re-emitted light. In the CB model inverse Compton scattering (ICS) of glory photons is the origin of the prompt γ /X-ray peaks, as we review in §3. Each peak is generated by a single CB emitted by the ‘engine’, the accreting compact object resulting from a core-collapse supernova event. We shall see that ICS correctly describes the prompt peaks, extending even into the optical domain in XRFs in which the relevant observations are available, such as XRF 060218. The natural explanation of the early time flares is the same as that of the stronger flares: ICS of glory photons by the electrons of CBs ejected in late accretion episodes of fall-back matter on the newly formed central object. These CB emissions must correspond to a weakening activity of the engine, as the accreting material becomes scarcer.

In the CB model, from the onset of the ‘plateau’ onwards, the X-ray, optical (DDD2002a) and radio (DDD2003a) afterglows are dominated by synchrotron radiation (SR), the CB-model predictions for which are reviewed in §4. On occasion these AGs also have transient

rebrightenings (‘very late’ flares), two notable cases before the Swift era being GRB 970508 (Amati et al. 1999, Galama et al. 1998a) and GRB 030329 (Lipkin et al. 2004). During these episodes, the spectrum continues to coincide with the one predicted on the basis of the synchrotron mechanism that dominates the late AGs. These very late flares are well described by encounters of CBs with density inhomogeneities in the interstellar medium (DDD2002a, DD2004). Very late flares in the *XUVONIR* AG may have this origin as well.

In this article we compare the predictions of the CB model and the observed X-ray and optical light curves of 33 selected GRBs, which are well sampled from very early time until late time, have a relatively long follow-up with good statistics and represent well the entire diversity of Swift GRBs. These include the brightest of the Swift GRBs (080319B), the GRB with the longest measured X-ray emission (060729), a few with canonical X-ray light curves (050315, 060526, 061121 and 080320) with and without superimposed X-ray flares, GRBs with semi-canonical light curves (060211A, 061110A, 070220, 080303, 080307, 051021B) and non-canonical light curves (061007, 061126, 060206), and some of the allegedly most peculiar GRBs (050319, 050820A, 060418, 060607A, 071010A, 061126). We also compare the CB model prediction and the observed X-ray light curve of additional 12 GRBs with the most rapid late-time temporal decay.

In the CB model, LGRBs and XRFs are one and the same, the general distinction being that XRFs are viewed at a larger angle relative to the direction of the approaching jet of CBs or have a relatively small Lorentz factor (DD2004, Dado et al. 2004c). Thus we include a Swift XRF of particular interest in our analysis: 060218. Its X-ray light curve is shown to be the normal X-ray light curve of a GRB viewed far off axis, and not the emission from the break-out of a spherical shock wave through the stellar envelope. Its optical AG at various frequencies shows, before the SN becomes dominant, a series of broad peaks between 30 ks and 60 ks after trigger, which we interpreted as the optical counterparts of the dominant prompt X-ray peak of this XRF. The expressions for an ICS-generated peak at all frequencies allow us to predict the positions, magnitudes and pulse shape of these broad peaks, a gigantic extrapolation in time, radiated energy and frequency.

After submitting for publication a first version of a comparison between the CB-model predictions and Swift observations (DDD2007c), we have compared many more Swift data with the CB-model predictions, in order to further test its ability to predict correctly all the main properties of GRB light curves. These included the rapid spectral evolution observed during the fast decay of the prompt emission in ‘canonical’ GRBs (DDD2008a) and the ‘missing AG breaks’ in the AG of several GRBs (DDD2008b). We have also extended the CB model to describe short hard bursts (SHBs) and confronted it with the entire data on all SHBs with well-measured X-ray and/or optical afterglows (Dado & Dar 2008).

Together with the GRBs discussed in this report, we have analyzed and published CB model fits to the light curves of more than 100 LGRBs and SHBs. The CB model continued to be completely successful in the confrontation of its predictions with the data.

2. The CB Model

In the CB model (e.g. DD2004 and references therein) *long-duration* GRBs and their AGs are produced by bipolar jets of CBs which are ejected (Shaviv & Dar, 1995, Dar & Plaga, 1999) in *ordinary core-collapse* supernova explosions¹. An accretion disk or a torus is hypothesized to be produced around the newly formed compact object, either by stellar material originally close to the surface of the imploding core and left behind by the explosion-generating outgoing shock, or by more distant stellar matter falling back after its passage (De Rújula 1987). As observed in microquasars (e.g. Mirabel & Rodriguez 1999, Rodriguez & Mirabel 1999 and references therein), each time part of the accretion disk falls abruptly onto the compact object, a pair of CBs made of *ordinary-matter plasma* with a typical baryonic number, $N_B \sim 10^{50}$, are emitted with large bulk-motion Lorentz factors, typically $\gamma_0 \sim 10^3$, in opposite directions along the rotation axis, wherefrom matter has already fallen back onto the compact object, due to lack of rotational support.

The γ -rays of a single pulse of a GRB are produced as a CB coasts through the SN *glory*, the light emitted and scattered by the ‘wind’ —the ejecta puffed by the progenitor star continuously or in a succession of pre-SN flares— after being illuminated by the progenitor’s pre-supernova and SN light. The electrons enclosed in the CB Compton up-scatter the photons of the glory to GRB energies. The initial fast expansion of the CBs and the increasing transparency of the wind environment as the CBs penetrates it, result in the fast rise of GRB pulses. As the CB coasts further through the SN glory, the density and temperature decrease rapidly. Consequently, the energy of the up-scattered photons is continuously shifted to lower energies and their number decreases rapidly. Typically, the ensuing fast decline of the prompt emission is taken over, within a couple of minutes of observer’s time, by a broad-band synchrotron emission from swept-in electrons from the wind and the interstellar medium (ISM) spiraling in the CB’s enclosed magnetic field.

¹Supernovae associated with GRBs are viewed uncommonly close to their jet axis, near which the non-relativistic ejecta from the SN are faster than average. The observed initial large velocities of the leading ejecta may, erroneously in our view, lead to their interpretation as a very special GRB-associated class of super energetic SNe: ‘*hypernovae*’. Yet, the velocities of their ejecta have been observed to decrease within a year or two after the explosion (before they have swept a significant amount of circumburst matter) to a typical 5000-7000 km s⁻¹, implying a normal SN kinetic energy release of a few times 10⁵¹ erg.

In the CB model there is no clear-cut *temporal* distinction between prompt and *afterglow* signals. There are, however, two rather distinct radiation mechanisms: inverse Compton scattering and synchrotron radiation. For all cases we have studied, the prompt emission of γ -rays, X-rays and optical light in XRFs is dominated by ICS whereas in ordinary GRBs, only the prompt emission of γ and X-rays is dominated by ICS, while SR dominates the prompt optical emission and the broad-band afterglow emission. Usually, the SR takes over the X-ray emission during the fast decay of the prompt emission or at the onset of the ‘plateau’ phase. Late flares appear to be dominated by SR.

3. Inverse Compton Scattering

3.1. The spectrum of ICS pulses

During the initial phase of γ -ray emission in a GRB, the Lorentz factor γ of a CB stays put at its initial value $\gamma_0 = \mathcal{O}(10^3)$, for the deceleration induced by the collisions with the ISM has not yet had a significant effect (DDD2002a, DDD2003a). Let θ be the observer’s angle relative to the direction of motion of a CB. The Doppler factor by which light emitted by a CB is boosted in energy is,

$$\delta = \frac{1}{\gamma(1 - \beta \cos \theta)} \approx \frac{2\gamma}{1 + \gamma^2 \theta^2}, \quad (1)$$

where the approximation is excellent for $\gamma \gg 1$ and $\theta \ll 1$. The emitted light is forward-collimated into a cone of characteristic opening angle $1/\gamma$, so that the boosted energetic radiation is observable for $\theta = \mathcal{O}(1/\gamma_0)$. This implies that the typical initial Doppler factor of a GRB is: $\delta_0 = \mathcal{O}(10^3)$.

The burst environment is very complex, and can only be roughly approximated. After it is ejected, the fast-expanding CB propagates through a cavity produced by the pre-supernova ejecta, and shortly encounters the previously ejected ‘windy environment’, whose density distribution is roughly $n(r) \propto 1/r^2$. The initially fast-expanding CB scatters the quasi-isotropic distribution of glory light and the collimated light from the CBs themselves². The glory light has a thin thermal bremsstrahlung spectrum

$$\epsilon \frac{dn_\gamma}{d\epsilon} \approx n_\gamma(r) \left(\frac{\epsilon}{kT_g} \right)^{-\beta_g} e^{-\epsilon/kT_g}, \quad (2)$$

²The CB arrives at the windy environment shortly after its emitted light, well before the scattered photons could have left the beaming cone, since $r/2c\gamma^2 \ll r/\gamma c$.

with $\beta_g \sim 0$ and a temperature that decreases with distance beyond a characteristic r_g like $T_g(r) \sim T(0) r_g^2 / (r_g^2 + r^2)$, with $k T(0) \sim 1$ eV. The observed energy of a glory photon which was scattered by an electron comoving with a CB at redshift z , is:

$$E = \frac{\gamma_0 \delta_0 \epsilon (1 + \cos \theta_{in})}{1 + z}, \quad (3)$$

where θ_{in} is the angle of incidence of the initial photon onto the CB, in the SN rest system. For a quasi-isotropic distribution of glory light, $\cos \theta_{in}$ in Eq. (3) roughly averages to zero. The predicted time-dependent spectrum of the GRB pulse produced by ICS of the glory photons is given by (DD2004):

$$E \frac{dN_\gamma}{dE} \sim \left(\frac{E}{E_p(t)} \right)^{-\beta_g} e^{-E/E_p(t)} + b(1 - e^{-E/E_p(t)}) \left(\frac{E}{E_p(t)} \right)^{-p/2}, \quad (4)$$

where

$$\begin{aligned} E_p(t) &\approx E_p(0) \frac{t_p^2}{t^2 + t_p^2}, \\ E_p(0) &\approx \frac{\gamma_0 \delta_0}{1 + z} k T_g(0), \end{aligned} \quad (5)$$

with $t_p \approx (1+z) r_g / c \gamma_0 \delta_0$, the peak time of dN_γ/dt , discussed in the next chapter.

The first term in Eq. (4), with $\beta_g \sim 0$, is the result of Compton scattering by the bulk of the CB's electrons, which are comoving with it. The second term in Eq. (4) is induced by a very small fraction of 'knocked-on' and Fermi-accelerated electrons, whose initial spectrum (before Compton and synchrotron cooling) is $dN_e/dE \propto E^{-p}$, with $p \approx 2.2$. For $b = \mathcal{O}(1)$, the energy spectrum predicted by the CB model, Eq. (4), bears a striking resemblance to the Band function (Band et al. 1993) traditionally used to model the energy spectra of GRBs, but GRBs whose spectral measurements extended over a much wider energy range than that of BATSE and Swift's BAT, are better fitted by Eq. 4 (e.g. Wigger et al. 2008).

For many Swift GRBs the spectral observations do not extend to energies bigger than $E_p(0)$, or the value of b in Eq. (4) is relatively small, so that the first term of the equation provides a very good approximation. But for its time-dependence, this term coincides with the 'cut-off power-law' which has also been recently used to model GRB spectra. For $b \sim 0$ and $\beta_g \sim 0$ it yields a peak value of $E^2 dN/dE$ at $E_p(t)$ whose pulse-averaged value is:

$$E_p \approx E_p(t_p) \approx 0.5 E_p(0) \approx 155 \frac{\gamma_0 \delta_0}{10^6} \frac{T(0)}{1 \text{ eV}} \frac{3.2}{1 + z} \text{ keV}, \quad (6)$$

where the numerical result was obtained for the pulse shape discussed in the next subsection and the indicated typical values, including the mean redshift $\langle z \rangle \approx 2.2$ of Swift's long GRBs

(Greiner: <http://www.mpe.mpg.de/~jcg/grbgen.html>). For $b=1$ and $\beta_g \sim 0$, E_p is larger by 50% than the result of Eq. (6). The predicted spectrum, Eq. (4), and the range of E_p values, Eq. (6), are in good agreement with the observations of BATSE, BeppoSAX, Konus-Wind, INTEGRAL, Suzaku and RHESSI, which cover a much broader energy range than Swift³.

In the CB model XRFs are either GRBs with typical values of γ_0 , but viewed from angles $\theta \gg 1/\gamma_0$, or GRBs with smaller γ_0 (DD2004, DDD2004a). Both choices imply a smaller δ_0 in Eq. (1), and consequently the softer spectrum and relatively small E_p that define an XRF, see Eqs. (4,5). XRFs have light curves with wider and less rugged peaks than GRBs. This follows from the time dependence of the light curves, which we discuss next.

3.2. The light curves of GRB and XRF pulses

After launch, as the CB propagates in the progenitor's wind on its way to the ISM, its cross section increases, its density and the wind's density decrease and consequently their opacities decrease. Let t be the time after launch of a CB as measured by a distant observer. Approximating the CB geometry by a cylindrical slab with the same radius, density and volume, and neglecting multiple scattering and the spread in arrival times of ICS photons from the CB which entered it simultaneously, their arrival rate is given by:

$$\frac{dN_\gamma}{dt} = e^{-\tau_w} n_g(t) \sigma_T \pi R^2(t) \frac{[1 - e^{-\tau_{CB}}]}{\sigma_a}, \quad (7)$$

where τ_w is the opacity of the wind at the CB location, τ_{CB} is the effective opacity of the expanding CB encountered by a photon with energy $E' = (1+z)E/\delta_0$ which begins crossing it at a time t , $\sigma_a(E')$ is the photo-absorption cross section at energy E' and σ_T is the Thomson cross section. The density of the glory photons seen by a CB is quasi isotropic and decreases roughly like $n_g \propto 1/(r^2 + r_g^2)$, where r_g is distance where the wind becomes transparent (optical thickness ~ 1) to glory photons. At an early time, $r \approx c\gamma_0\delta_0 t/(1+z)$. Consequently $n_g \propto 1/(t^2 + \Delta t^2)$, where $\Delta t = (1+z)r_g/c\gamma_0\delta_0$. Thus the shape of an ICS pulse produced by a CB is given approximately by

$$E \frac{d^2 N_\gamma}{dt dE} \propto e^{-\tau_w} n_g \pi R^2 [1 - e^{-R_{tr}^2/R^2}] E \frac{dN_\gamma}{dE}, \quad (8)$$

where R_{tr} is the radius of the CB at $t=t_{tr}$, when $\tau_{CB} \approx 1$, i.e., when it becomes transparent to the scattered radiation, and $E dN_\gamma/dE$ is given by Eq. (4). The pre-supernova wind from

³Swift data can determine E_p only when it is well within its 15-350 keV detection range. This results in a biased sample of GRBs whose *measured* E_p is smaller than the average over the entire GRB population.

the progenitor star produces a density distribution, $n(r) = n_0 r_0^2 / r^2$ around it, which yields $\tau_w = a(E)/t$ with $a(E) = \sigma_a n_0 r_0^2 (1+z)/c \gamma_0 \delta_0$. At sufficiently high energies the opacities of the wind and the CBs are mainly due to Compton scattering and $R_{tr} \sim \sqrt{\sigma_T N_B / \pi}$, where σ_T is the Thomson cross section and N_B is the baryon number of the expanding CB. At low energies, their opacity is dominated by free-free absorption because the CBs and the wind along their trajectory are completely ionized. In the CBs' rest frame the glory photons have typical energies, $E' \ll \text{keV}$. At such low energies, the opacity of CBs with a uniform density behaves like $\tau_{CB} \sim E'^{-3} (1 - e^{-E' k / T'}) G(E') R^{-5}$, where $G(E')$ is the quantum mechanical Gaunt factor that depends logarithmically on E' (e.g. Lang 1980 and references therein). Thus, when the optical thickness of a CB is dominated by free-free photo-absorption, its transparency radius increases with decreasing energy like $R_{tr} \propto E^{-3/5} = E^{-0.6}$ at $E' \gg k T'$ and $R_{tr} \propto E^{-2/5} = E^{-0.4}$ at $E' \ll k T'$, yielding $R_{tr} \sim E^{-0.5 \pm 0.1}$.

The initially rapid expansion of a CB slows down as it propagates through the wind and scatters its particles (DDD2002, DD2004). This expansion may be roughly described by $R^2 \approx R_{cb}^2 t^2 / (t^2 + t_{exp}^2)$, where R_{cb} is the asymptotic radius of the CB and $t_{exp} \gg t_{tr}$. Thus, Eq. (8) can be approximated by

$$E \frac{d^2 N_\gamma}{dt dE} \propto \frac{e^{-a/t} \Delta t^2 t^2}{(t^2 + \Delta t^2)(t^2 + t_{tr}^2)} E \frac{dN_\gamma}{dE}. \quad (9)$$

For nearly transparent winds ($a \rightarrow 0$) and for $t_{tr} \sim \Delta t$, Eq. (9) has an approximate shape

$$E \frac{d^2 N_\gamma}{dt dE} \propto \frac{\Delta t^2 t^2}{(t^2 + \Delta t^2)^2} E \frac{dN_\gamma}{dE}, \quad (10)$$

which peaks around $t \approx \Delta t$. Except for very early times, this shape is almost undistinguishable from that of the ‘Master’ formula of the CB model (DD2004):

$$E \frac{d^2 N_\gamma}{dt dE} \propto e^{-\Delta t^2 / t^2} [1 - e^{-\Delta t^2 / t^2}] E \frac{dN_\gamma}{dE}, \quad (11)$$

which also took into account arrival-time effects that depend on the geometry of the CB and the observer's viewing angle, and was shown to describe well the prompt emission pulses of LGRBs (DD2004) and their rapid decay with a fast spectral softening (DDD2008a).

At the relatively low X-ray energies covered by Swift and, more so, at smaller ones, the first term on the RHS of Eq. (4) usually dominates $E dN_\gamma / dE$. Thus the light curve generated by a sum of ICS pulses at a luminosity distance D_L is generally well described by:

$$E \frac{d^2 N_\gamma}{dt dE} \approx \sum_i A_i \Theta[t - t_i] \frac{\Delta t_i^2 (t - t_i)^2}{((t - t_i)^2 + \Delta t_i^2)^2} e^{-E/E_{p,i}[t-t_i]}, \quad (12)$$

where the index ‘i’ denotes the i-th pulse produced by a CB launched at an observer time $t=t_i$, or, alternatively,

$$E \frac{d^2 N_\gamma}{dt dE} \approx \sum_i A_i \Theta[t-t_i] e^{-\Delta t_i^2/(t-t_i)^2} [1 - e^{-\Delta t_i^2/(t-t_i)^2}] e^{-E/E_{p,i}[t-t_i]}, \quad (13)$$

where $E_{p,i}[t-t_i]$ is given by Eq. (5) with t replaced by $t-t_i$ and

$$A_i \approx \frac{c n_g(0) \pi R_{CB}^2 \gamma_0 \delta_0^3 (1+z)}{4 \pi D_L^2}. \quad (14)$$

Thus, in the CB model, each ICS pulse in the GRB light curve is effectively described by four parameters, t_i , A_i , Δt_i and $E_{p,i}(0)$, which are best fitted to reproduce its observed light curve. The evolution of its peak energy is then determined.

Setting $t_i = 0$, $E_p(t)$ has the approximate form $E_p(t) \approx E_p t_p^2 / (t_p^2 + t^2)$. Such an evolution has been observed in the time-resolved spectrum of well-isolated pulses (see, for instance, the insert in Fig. 8 of Mangano et al. 2007), until the ICS emission is overtaken by the broad-band synchrotron emission from the swept-in ISM electrons. Hence, the temporal behaviour of the separate ICS peaks is given by:

$$E \frac{d^2 N_\gamma}{dt dE}(E, t) \propto \frac{t^2 / \Delta t^2}{(1 + t^2 / \Delta t^2)^2} e^{-E t^2 / E_p t_p^2} \approx F(E t^2), \quad (15)$$

to which we shall refer as the ‘ $E t^2$ law’. A simple consequence of this law is that unabsorbed ICS peaks have approximately identical shape at different energies when their $E d^2 N_\gamma / dt dE$ is plotted as a function of $E t^2$.

A few other trivial but important consequences of Eq. (15) for unabsorbed GRB peaks at $E \lesssim E_p$ are the following:

- The peak time of a pulse is at

$$t_p = t_i + \Delta t_i. \quad (16)$$

- The full width at half maximum (FWHM) of a pulse is

$$\text{FWHM} \approx 2 \Delta t_i, \quad (17)$$

and it extends from $t \approx t_i + 0.41 \Delta t_i$ to $t \approx t_i + 2.41 \Delta t_i$.

- The rise time (RT) from half peak value to peak value satisfies

$$\text{RT} \approx 0.30 \text{ FWHM}, \quad (18)$$

independent of energy. This result agrees with the empirical relation that was inferred by Kocevski et al. (2003) from bright BATSE GRBs, $\text{RT} \approx (0.32 \pm 0.06) \text{ FWHM}$.

- The FWHM increases with decreasing energy approximately like a power-law:

$$\text{FWHM}(E) \sim E^{-0.5}. \quad (19)$$

This relation is consistent with the empirical relation $\text{FWHM}(E) \propto E^{-0.42 \pm 0.06}$, satisfied by BATSE GRBs (Fenimore et al. 2003).

- The onset-time, t_i , of a pulse is simultaneous at all energies. But the peak times t_p at different energies differ, the lower-energy ones ‘lagging’ behind the higher-energy ones:

$$t_p - t_i \propto E^{-0.5}. \quad (20)$$

- The time-averaged value of $E_p(t)$ for GRB peaks, which follows from Eq. (5), satisfies:

$$E_p = E_p(0)/2 = E_p(t_p). \quad (21)$$

3.3. X-ray ‘flares’ and γ -ray pulses

In more than 50% of the GRBs observed by Swift, the X-ray light curve, during the prompt GRB and its early AG phase, shows flares superimposed on a smooth background. In the CB model, an X-ray ‘flare’ coincident in time with a γ -ray pulse is simply its low-energy tail. Both are due ICS of photons in the thin-bremsstrahlung glory. The glory’s photons incident on the CB at small ϵ_i or $1+\cos\theta_i$ result in X-ray or softer up-scattered energies, see Eq. (3). The harder and less collinear photons result in γ -rays. The light curve and spectral evolution of an ICS X-ray flare are given approximately by Eq. (12). Its width is related to that of the accompanying γ -ray pulse as in Eq. (17). Relative to its γ -ray counterpart, an X-ray flare is wider and its peak time ‘lags’ after the peak time of the γ -ray pulse. The X-ray flares during a GRB are well separated only if the γ -pulses are sufficiently spaced.

In the CB model, X-ray flares without an accompanying detectable γ -ray emission can be of two kinds. They can be ICS flares produced by CBs ejected with relatively small Lorentz factors and/or relatively large viewing angles (Dado et al. 2004). Such CBs may be ejected in accretion episodes both during the prompt GRB and in delayed accretion episodes onto the newly formed central object in core collapse SNe (De Rújula 1987). ICS flares satisfy the $E t^2$ -law and exhibit a rapid softening during their fast decline phase which is well described by Eqs. (4,5), as shown in detail in DDD2008b.

We shall see in our case studies that very often, during the rapidly decreasing phase of the prompt emission, there are ‘mini X-ray flares’ which show this rapid spectral softening. As

the accretion material is consumed, one may expect the ‘engine’ to have a few progressively-weakening dying pangs.

Flares can also be due to enhanced synchrotron emission during the passage of CBs through over-densities produced by mass ejections from the progenitor star or by interstellar winds (DDD2002a, DDD2003a). The synchrotron emission from CBs is discussed in the following section. Late flares seem to have the predicted synchrotron spectrum and spectral evolution which are different from those of ICS flares.

4. Synchrotron radiation

A second mechanism besides ICS, which generates radiation from a CB, is synchrotron radiation (SR). A CB encounters matter in its voyage through the interstellar medium (ISM), effectively ionized by the high-energy radiation of the very same CB. This continuous collision with the medium decelerates the CB in a characteristic fashion, and results in a gradual steepening of the light curves of their emitted synchrotron radiation (DDD2002a). In §4.1, we review the calculation of $\gamma(t)$, the CB’s diminishing Lorentz factor. We have assumed and tested observationally, via its CB-model consequences, that the impinging ISM generates within the CB a turbulent magnetic field⁴, in approximate energy equipartition with the energy of the intercepted ISM (DDD2002a, DDD2003a). In this field, the intercepted electrons emit synchrotron radiation. This radiation, isotropic in the CB’s rest frame, is Doppler boosted and collimated around the direction of motion into a cone of characteristic opening angle $\theta(t) \sim 1/\gamma(t)$. In §4.2 we summarize the predictions of the synchrotron radiation’s dependence on time and frequency (DDD2002a, DDD2003a).

4.1. The deceleration of a CB

As it ploughs through the ionized ISM, a CB gathers and scatters its constituent ions, mainly protons. These encounters are ‘collisionless’ since, at about the time it becomes transparent to radiation, a CB also becomes ‘transparent’ to hadronic interactions (DD2004). The scattered and re-emitted protons exert an inward pressure on the CB, countering its expansion. In the approximation of isotropic re-emission in the CB’s rest frame and a

⁴‘First principle’ numerical simulations of two plasmas merging at a relative relativistic Lorentz factor (Frederiksen et al. 2003, 2004, Nishikawa et al. 2003) do not generate the desired shocks, but do generate turbulently moving magnetic fields.

constant ISM density $n \sim n_e \sim n_p$, one finds that within minutes of observer’s time t , a typical CB of baryon number $N_B \approx 10^{50}$ reaches a roughly constant ‘coasting’ radius $R \sim 10^{14}$ cm, before it finally stops and blows up, after a journey of years of observer’s time. During the coasting phase, and in a constant-density ISM, $\gamma(t)$ obeys (DDD2002a, Dado et al. 2006):

$$(\gamma_0/\gamma)^{3+\kappa} + (3 - \kappa) \theta^2 \gamma_0^2 (\gamma_0/\gamma)^{1+\kappa} = 1 + (3 - \kappa) \theta^2 \gamma_0^2 + t/t_0, \quad (22)$$

with

$$t_0 = \frac{(1+z) N_B}{(6+2\kappa) c n \pi R^2 \gamma_0^3}, \quad (23)$$

where the numerical value $\kappa=1$, is for the case in which the ISM particles re-emitted fast by the CB are a small fraction of the flux of the intercepted ones, and $\kappa=0$ in the opposite limit. In the CB model of cosmic rays (Dar & De Rújula 2006) the observed spectrum strongly favours $\kappa=1$. Thus in all of our fits we use $\kappa=1$, though the results are not decisively sensitive to this choice. As can be seen from Eq. (22), γ and δ change little as long as $t < t_b = [1 + \gamma_0^2 \theta^2]^2 t_0$. where, in terms of typical CB-model values of γ_0 , R , N_B and n ,

$$t_b = (1300 \text{ s}) [1 + \gamma_0^2 \theta^2]^2 (1+z) \left[\frac{\gamma_0}{10^3} \right]^{-3} \left[\frac{n}{10^{-2} \text{ cm}^{-3}} \right]^{-1} \left[\frac{R}{10^{14} \text{ cm}} \right]^{-2} \left[\frac{N_B}{10^{50}} \right]. \quad (24)$$

For $t \gg t_b$, γ and δ decrease like $t^{-1/4}$.

The deceleration equation for a non-expanding CB can be integrated analytically also for other commonly encountered density profiles, such as a step function times $n(r) \propto 1/r^2$. Such a profile is produced by a constantly blowing wind from a massive progenitor star prior to the GRB, or from a star formation region, or in an isothermal sphere which describes quite well the density distribution in galactic bulges, galactic halos and elliptical galaxies.

4.2. The Synchrotron spectral energy density

As indicated by first-principle calculations of the relativistic merger of two plasmas (Frederiksen et al. 2004), the ISM ions continuously impinging on a CB generate within it turbulent magnetic fields, which we assume to be in approximate energy equipartition with their energy, $B \approx \sqrt{4\pi n m_p c^2} \gamma$. In this field, the intercepted electrons emit synchrotron radiation. The SR, isotropic in the CB’s rest frame, has a characteristic frequency, $\nu_b(t)$, the typical frequency radiated by the electrons that enter a CB at time t with a relative Lorentz factor $\gamma(t)$. In the observer’s frame:

$$\nu_b(t) \simeq \frac{\nu_0}{1+z} \frac{[\gamma(t)]^3 \delta(t)}{10^{12}} \left[\frac{n}{10^{-2} \text{ cm}^3} \right]^{1/2} \text{ Hz}. \quad (25)$$

where $\nu_0 \simeq 3.85 \times 10^{16}$ Hz $\simeq 160$ eV/h. The spectral energy density of the SR from a single CB at a luminosity distance D_L is given by (DDD2003a):

$$F_\nu \simeq \frac{\eta \pi R^2 n m_e c^3 \gamma(t)^2 \delta(t)^4 A(\nu, t)}{4 \pi D_L^2 \nu_b(t)} \frac{p-2}{p-1} \left[\frac{\nu}{\nu_b(t)} \right]^{-1/2} \left[1 + \frac{\nu}{\nu_b(t)} \right]^{-(p-1)/2}, \quad (26)$$

where $p \sim 2.2$ is the typical spectral index⁵ of the Fermi-accelerated electrons, $\eta \approx 1$ is the fraction of the impinging ISM electron energy that is synchrotron re-radiated by the CB, and $A(\nu, t)$ is the attenuation of photons of observed frequency ν along the line of sight through the CB, the host galaxy (HG), the intergalactic medium (IGM) and the Milky Way (MW):

$$A(\nu, t) = \exp[-\tau_\nu(\text{CB}) - \tau_\nu(\text{HG}) - \tau_\nu(\text{IGM}) - \tau_\nu(\text{MW})]. \quad (27)$$

The opacity $\tau_\nu(\text{CB})$ at very early times, during the fast-expansion phase of the CB, may strongly depend on time and frequency. The opacity of the circumburst medium [$\tau_\nu(\text{HG})$ at early times] is affected by the GRB and could also be t - and ν -dependent. The opacities $\tau_\nu(\text{HG})$ and $\tau_\nu(\text{IGM})$ should be functions of t and ν , for the line of sight to the CBs varies during the AG observations, due to the hyperluminal motion of CBs.

The dependence of the SR afterglow on the CB's radius, external density and extinction, as summarized in Eq. (26), give rise to a variety of early-time optical light curves, in contrast to the more uniform behaviour of the optical and X-ray SR afterglow at later times.

4.3. The X-ray afterglow

The Swift X-ray band is usually above the bend frequency ν_b , as given by Eq. (25), at all times. It then follows from Eq. (26) that the spectral energy density of the *unabsorbed* X-ray afterglow has the form:

$$F_\nu \propto R^2 n^{(p+2)/4} \gamma^{(3p-2)/2} \delta^{(p+6)/2} \nu^{-p/2} = R^2 n^{\Gamma/2} \gamma^{3\Gamma-4} \delta^{\Gamma+2} \nu^{-\Gamma+1}, \quad (28)$$

where we have used the customary notation $dN_\gamma/dE \propto E^{-\Gamma}$.

The deceleration of a CB causes a transition of its γ and δ values from being approximately constant to asymptotic power-law declines. For a constant ambient density this

⁵The normalization in Eq. (25) is only correct for $p > 2$, for otherwise the norm diverges. The cutoffs for the ν distribution are time-dependent, dictated by the acceleration and SR cooling times of electrons and their 'Larmor' limit. The discussion of these processes being complex (DD2003a, DD2006), we shall satisfy ourselves here with the statement that for $p \leq 2$ the AG's normalization is not predicted.

occurs gradually around $t=t_b$ and the asymptotic decline is $\delta \propto \gamma \propto t^{-1/4}$, see Eq.(24). This induces a gradual *bend* (usually called a “break”) in the synchrotron AG of a CB from a plateau to an asymptotic power-law decay

$$F_\nu \propto t^{-p/2-1/2} \nu^{-p/2} = t^{-\Gamma+1/2} \nu^{-\Gamma+1}, \quad (29)$$

with a power-law in time steeper by half a unit than that in frequency. For a constant ISM density and in an often used notation, the asymptotic behaviour $F_\nu(t) \propto t^{-\alpha} \nu^{-\beta}$, satisfies

$$\alpha = \beta + 1/2 = p/2 + 1/2 = \Gamma - 1/2. \quad (30)$$

For a fast-falling density beyond a given distance r_c , crossed by CBs exiting density enhancements due to stellar winds or by CBs which escape the galactic bulge or disk into the galactic halo, γ and δ tend to approximately constant values. Consequently $r-r_c$ becomes proportional to $t - t_c \equiv t - t(r_c)$. As a result, for a density profile such as $n \propto 1/r^2$ beyond r_c , the unattenuated synchrotron afterglow, as given by Eq. (28), approximately tends to

$$F_\nu \propto n^{(p+2)/4} \nu^{-p/2} \propto (t - t_c)^{-(p+2)/2} \nu^{-p/2} = (t - t_c)^{-\Gamma} \nu^{-\Gamma+1}, \quad (31)$$

and satisfies the asymptotic relation

$$\alpha = \beta + 1 = \Gamma \approx 2.1. \quad (32)$$

Thus, an unattenuated optical and X-ray AG may steepen at late times to an asymptotic decline $\sim (t - t_c)^{-2.1}$. Such an achromatic steepening, which was seen in several late-time optical and X-ray AGs of Swift GRBs (see Figs. 6,7), may have been misinterpreted as very late ‘jet breaks’ (e.g. Dai et al. 2008, Racusin et al. 2008a).

All of the afterglows of Swift GRBs which are well sampled at late time satisfy one or the other of the asymptotic relations (30) or (32) (DDD2008b).

4.4. Early-time SR

During the early-time when both γ and δ stay put at their initial values γ_0 and δ_0 , Eq. (26) yields a SR light curve $F_\nu \propto e^{-\tau_w} R^2 n^{(1+\beta)/2} \nu^{-\beta}$. Since $r \propto t$, a CB ejected into a windy density profile $n \propto 1/r^2$, created by the mass ejection from the progenitor star prior to its SN explosion, emits SR with an early-time light curve of the form

$$F_\nu \propto \frac{e^{-a/t} t^{1-\beta}}{t^2 + t_{exp}^2} \nu^{-\beta}, \quad (33)$$

where, for a CB ejected at time t_i , t must be replaced by $t - t_i$.

In the γ -ray and X-ray bands, the SR emission from a CB is usually hidden under the prompt ICS emission. But in many GRBs the asymptotic exponential decline of the energy flux density of the prompt ICS emission, $F_\nu \propto t^{-2} e^{-E t^2/E_p t_p^2}$, is taken over by the slower power-law decline, $F_\nu \propto t^{-\Gamma}$, of the synchrotron emission in the windy $\sim 1/r^2$ circumburst density before the CB reaches the constant ISM density and the AG emission enters the plateau phase. This is demonstrated in Fig. 3 for GRBs 051021B, 060211A, 061110A, 070220, 080303, 080307. As soon as the light curve is dominated by SR, the rapid spectral softening of the ICS-dominated light curve stops and the spectrum of the unabsorbed X-ray emission changes to the ordinary synchrotron power-law spectrum with the typical power-law index, $\beta_X \approx 1.1$ ($\Gamma \approx 2.1$). Unlike the sudden change in the spectrum when the prompt ICS emission is taken over by SR during the plateau phase, there is no spectral change when SR dominates the X-ray light curve already before the plateau phase.

When the windy density profile changes to a constant ISM density, the light curve of the early-time optical AG, as given by Eq. (33), changes to a plateau or a shallow decline with a typical SR optical spectrum. After the deceleration bend, the temporal decline of the optical AG begins to approach that of the X-ray AG because the bend frequency, which decreases like $\nu_b \propto \sqrt{n} \gamma^3 \delta$, moves below the optical band. After the cross-over, $\beta_O(t) \approx \beta_X \approx 1.1$ and the AG becomes achromatic, approaching the asymptotic power-law decay $F_\nu \sim t^{-\beta_X - 1/2}$, and yielding an optical AG with a similar early and late power-law decline, $F_\nu \sim t^{-1.6}$. This behaviour has been observed in several very bright GRBs whose optical light curve was discovered early enough and was followed until late time, e.g. in GRBs 990123, 021211, 061007, 061126 and 080319B (see Fig. 2). Unlike the prompt γ -ray and X-ray emission in ordinary GRBs, which is dominated by ICS, their prompt optical emission is dominated by SR. This is because $F_\nu[\text{SR}]$ increases with decreasing frequency like $\nu^{-\beta_O}$ with $\beta_O \sim 0.5$, whereas the prompt ICS emission for $h\nu \ll E_p$ is independent of frequency ($\beta \approx 0$).

The entire diversity of the chromatic early-time optical light curves of LGRBs measured with robotic telescopes, such as GRBs 030418 (Rykoff et al. 2004), 050319 (Wozniak et al. 2005, Quimby et al. 2006a), 050820A (Cenko et al. 2006, Vestrand et al. 2006), 060418 (Molinari et al. 2007) 060605 (Ferrero et al. 2008), 060607A (Molinari et al. 2007, Nysewander et al. 2007, Ziaepour et al. 2008), 071010A (Covino et al. 2008), and 061126 (Perley et al. 2008; Gomboc et al. 2008), is described well by Eq. (33). This is shown in Figs. 5,8.

The early SR obeys $F_\nu \propto \gamma_0^{3\beta-1} \delta_0^{3+\beta}$. Unlike ordinary GRBs with large $\delta_0 \sim \gamma_0$, XRFs are GRBs with a relatively small $\delta_0 \sim \gamma_0$ (near-axis XRFs) or far off-axis GRBs with $\delta_0 \ll \gamma_0$. Consequently, the prompt optical emission in XRFs is also dominated by ICS. An optical pulse that is dominated by ICS emission is distinguishable from an optical pulse that is

dominated by SR, in shape, spectrum and spectral evolution. Optical peaks produced by ICS satisfy the approximate $E t^2$ law, they are much wider than their γ -ray and X-ray counterparts and, as a result, they are usually blended. In XRFs such as 060218 and 080109, however, the ICS optical peaks have a large lagtime and are clearly visible as humps in the light curves at different optical wavelengths, see Fig. 9.

4.5. Chromatic Afterglows

The early-time light curves of LGRBs are very chromatic because their prompt γ -ray and X-ray emission is dominated by ICS, while their optical emission is dominated by SR with entirely different temporal and spectral properties. Even in XRFs, where the prompt optical emission is also dominated by ICS, the light curves are very chromatic because the ICS pulses, which satisfy the ‘ $E t^2$ law’, are by themselves very chromatic, see Figs. 9,10.

The afterglow emission in GRBs is dominated by SR at all wavelengths. In XRFs the situation is more interesting: the same statement is not correct, should one adhere to the traditional definition of AG as anything seen after the decline of the prompt X- or γ - signal. This is discussed in detail in §5.1.8 on XRF 060218. The observed chromatic behaviour of the AGs results from their dependence on the circumburst density, the bend frequency and the attenuation of light along the line of sight to the source of the AG. The most general behaviour –that takes into account light attenuation inside the CBs and in the circumburst environment, CB expansion and density variation as summarized in Eq. (26), and the chromatic light curves of superimposed flares– is rather complex and will not be discussed in detail in this paper. The behaviour becomes simpler when the CB and circumburst medium become transparent to radiation and the fast expansion of the CB has slowed down.

For a constant circumburst density, the simplest situation arises when all observed frequencies are above the injection bend. Notice that for typical reference parameters, $\nu_b(0)$ in Eq. (25) corresponds to an energy well above the *UVO* bands. But there are cases where δ is sufficiently small, such as XRFs and GRBs with very small E_{iso} , and/or where n is very small, such that $\nu_b(0) \propto \sqrt{n} \gamma_0^3 \delta_0$, is already below the *UVO* bands. In that case the (unattenuated) synchrotron spectrum is $F_\nu \sim \nu^{-p/2}$, achromatic all the way from the *UVO* bands to X-ray band at all times, see Eq. (26).

In ordinary GRBs, $\nu_b(0)$ in Eq. (25) is usually well above the *UVO* bands, but below the X-ray band. In that case, the unabsorbed spectrum of the optical AG evolves in a predicted fashion from $F_\nu \propto [\nu/\nu_b(t)]^{-1/2}$ to $F_\nu \propto [\nu/\nu_b(t)]^{-p/2}$, the behaviour of the unabsorbed X-ray AG. Many cases of this very specific chromatic evolution have been studied in DDD2003a.

The success of their CB-model description corroborates the assumption that the CB’s inner magnetic-field intensity $B(t)$, of which $\nu_b(t)$ is a function, is approximately determined by the equipartition hypothesis.

In a constant density, the CBs begin to decelerate rapidly around the time t_b of Eq. (24). Thus, the bend frequency, $\nu_b(t) \propto \gamma^3 \delta$, declines rapidly with time beyond t_b and crosses below the optical band. According to Eqs. (24, 26), F_ν steepens around t_b to an asymptotic achromatic power-law decline, $F_\nu \propto \nu^{-\beta} t^{-\alpha}$ with $\alpha \approx \beta + 1/2 = \Gamma - 1/2$, all the way from X-rays to the *UVO* bands. This smooth CB-deceleration bend in the AG of canonical GRBs, beyond which the *XUVO* AG becomes achromatic, is not to be confused with the achromatic *break* predicted in fireball models (Rhoads 1997, 1999). The CB-model interpretation of this well understood achromatic bend-time (see, e.g. DDD2003a) is further strengthened by the facts that it is observed at the predicted time scale and displays the predicted correlations with the prompt GRB emission (DDD 2008b), and that the predicted asymptotic relations between the temporal and spectral power-law declines beyond it are well satisfied.

A variation of the chromatic behaviour due to bend-frequency crossing occurs when it happens early enough for the circumburst density profile to be still dominated by the progenitor’s pre-SN wind emissions. At early times, $t \ll t_b$, the deceleration of CBs has not significantly affected their motion and $\gamma(t)$ and $\delta(t)$ are practically constant. Yet, the observer’s bend frequency, $\nu_b(t) \propto \sqrt{n(t)} [\gamma(t)]^3 \delta(t)$, decreases with time as $n(t)$ varies. Keeping track of the n -dependence, we concluded (DDD2003a) from Eqs. (25,26) that the unattenuated early synchrotron radiation of a CB moving in a windy density profile, $n \sim r^{-2} \sim t^{-2}$, is given approximately by

$$F_\nu \propto n^{(1+\beta)/2} \nu^{-\beta} \propto t^{-(1+\beta)} \nu^{-\beta}. \quad (34)$$

In cases for which $\nu_b(0)$ is initially well above the *UVOIR* bands, $\beta \approx 0.5$, and the initial *UVOIR* behaviour is $F_\nu \propto t^{-1.5} \nu^{-0.5}$, while the X-ray AG, for which $\nu_b \ll \nu$ and $\beta \simeq 1.1$, behaves like $F_\nu \propto t^{-2.1} \nu^{-1.1}$ (DDD2003b). If the density continues to decline like $1/r^2$, then the bend frequency crosses below the *UVOIR* band, and the *XUVOIR* AG becomes achromatic with $\alpha \approx \beta + 1 = \Gamma \sim 2.1$.

Optical light curves with an early-time power-law decay, $F_\nu \sim t^{-1.5}$, have been observed, e.g. in GRB 990123 (Akerlof et al. 1999); GRB 021211 (Li et al. 2003) and GRB 061126 (Perley et al. 2008). Usually, the steeper $F_\nu \sim t^{-(1+\beta_x)} \sim t^{-2.1}$ early-time decline of the X-ray synchrotron emission is hidden under the dominant early-time ICS emission, but in several GRBs it is visible as a power-law tail that takes over the initial exponential decay of the ICS pulse, see Fig. 3. This take-over also stops the fast spectral softening of the ICS-dominated light curve and changes the soft spectrum into the harder SR spectrum.

In the CB model the absorption and extinction in the host galaxy, which are frequency

dependent, can also be time dependent even far from the burst environment. In a day of the highly aberrated observer’s time, CBs typically move to a few hundred parsecs from their birthplace, a region wherein the ionization should have drastically diminished and the line of sight to the CBs in the host and IGM has shifted considerably. Indeed, Watson et al. (2007) found very different X-ray-to-optical column density ratios in GRB afterglows. A strong variation in extinction at early times was observed, e.g. by Perley et al. (2008) in GRB 061126, and by Ferrero et al. (2008) in GRB 060605. A time-dependent IGM absorption was reported by Hao et al. (2007), but see also Thöne et al. (2008a). A frequency-dependent extinction and absorption, which change in the host galaxy with the line of sight to the moving CB, can change an intrinsically achromatic AG into an observed chromatic AG.

Finally, ICS, which dominates also the prompt optical emission in XRFs, results in a very specific chromatic behaviour: the X-ray light curve is declining rapidly, while the optical light curves are stretched by the $E t^2$ law and display humps that are nothing but the X-ray pulse(s) with their peak time and width stretched by the same law. A striking example is shown in Figs. 9 and 10 for XRF 060218, discussed in great detail in §5.1.

Because of the complex chromatic behaviour of GRB afterglows, we have limited our discussion to the chromatic properties of the AG of a single CB. The actual situation can be even more convoluted because the AG, like the prompt emission, is usually the sum of the contributions from many individual CBs ejected at slightly different times with different parameters (baryon number, Lorentz factor and emission angle) which have or have not merged by the time of the AG phase. For the sake of simplicity, brevity and predictivity, we shall assume that the AG from the entire ensemble of CBs can be calculated as if it was due to one or at most two effective CBs during the AG. Despite this simplification, the CB model, as we shall show, can reproduce and explain well, within observational uncertainties, the entire diversity of the measured light curves of the Swift GRBs and their afterglows.

5. Comparison with observations

To date, Swift has detected over 350 long GRBs, localized them through their γ , X-ray and *UVO* emissions and followed most of them until they faded into the background. Beside the Swift observations, there have been many prompt optical measurements of Swift GRBs by an increasing number of ground-based robotic telescopes, and follow-up measurements by other ground-based optical telescopes, including some of the largest ones. Incapable of discussing all Swift GRBs, we discuss only a sample of 33 of them (some 10% of all Swift GRBs), which have well sampled X-ray and optical light curves from early to late time, and which represent well the entire diversity of Swift GRBs.

We fit the X-ray light curves reported in the Swift/XRT GRB light curve repository: http://www.swift.ac.uk/xrt_curves/; Evans et al. (2007). We used Eq. (12) or Eq. (13) for the early-time ICS contribution, and Eq. (26) for the SR afterglow with its simple explicit limit, Eq. (33), for the very-early-time synchrotron emission. The a-priori unknown parameters are the number of CBs, their ejection time, baryon number, Lorentz factor and viewing angle and the environmental ones along the CBs’ trajectory, i.e. the distributions of the glory’s light and of the ISM density. To demonstrate that the CB model correctly describes all of the observed features of the Swift X-ray observations, it suffices to include in the fits only the main or the latest few observed pulses or flares in the prompt emission. This is because the exponential factor in Eq. (12) suppresses very fast the relative contribution of the earlier pulses by the time the data sample the later pulses or flares. It also suffices to fix the glory’s light and ISM density distribution to be the same along the trajectories of all CBs in a given GRB. The pulse shapes are assumed to be universal: given by Eq. (12). For the synchrotron contribution, in most cases it suffices to consider a common emission angle θ and an average initial Lorentz factor γ_0 for the ensemble of CBs.

The ISM density along the CBs’ trajectories was generally taken to have a windy contribution ($\propto 1/r^2$) near the ejection site, changing later to a constant ISM density. The windy density is only relevant in some optical synchrotron-dominated AGs for which very early data are available, as discussed in the previous section. Density bumps with a density decline $n \propto 1/r^2$ were assumed to generate X-ray and optical flares in the synchrotron emission at late times (DDD2003). Only for a small fraction of cases (~ 14 out of 350 Swift GRBs) the observed late-time decline could not be well fit unless a transition from a constant density to a density proportional to $1/r^2$ was assumed.

Case by case, the X-ray and optical light curves were calculated with the same CB parameters. The spectral index p of the Fermi-accelerated electrons in the CBs was treated as a free parameter. In the CB model it determines both the spectral and temporal declines of the AG, as in Eq. (26). In cases where the fit was insensitive to p we fixed its value to be the canonical one: $p=2.2$ (DDD2002). The relative normalization of the X-ray and optical AGs was generally treated as a free adjustable parameter except when both extinction of the optical light and absorption of the emitted X-rays could be estimated reliably. In such cases the predicted dependence on frequency could be tested. These favourable cases include prompt ICS flares and the late-time SR afterglow where both the X-ray band and the optical band are above the bend frequency and the SR afterglow becomes ‘achromatic’. No attempt was made to derive the environmental parameters, because the use of simplifying assumptions –the single-CB approximation and the lack of exact knowledge of the extinction of the optical radiation in the host galaxy– make such attempts potentially unreliable.

In the following case studies of a representative sample of the entire diversity of Swift GRBs, we include GRBs with canonical, non-canonical and semi-canonical light curves, with or without superimposed flares, GRBs with very chromatic early-time afterglows, GRBs with exceptionally rapidly decaying late afterglows and GRBs with very complex and chromatic light curves. Special attention is given to XRF 060218. The parameters used in the CB-model description of the ICS flares and the synchrotron afterglow of all the GRBs and XRFs to be discussed anon are listed in Tables 1 and 2.

5.1. Case studies

5.1.1. GRBs with a canonical X-ray light curve

GRB 060729. *X-ray observations:* This GRB is described and discussed in detail in Grupe et al. (2007). It was detected and located by Swift at UT 19:12:29 July 29, 2006 (Grupe et al. 2007). It is one of the brightest Swift GRB in X-rays and has the longest follow-up observations in X-rays: more than 125 days after burst. The X-ray observations were triggered by the detection of a GRB precursor by the BAT, which dropped into the background level within 6 s. Two other major overlapping peaks were detected 70 s after trigger and a fourth one around 120 s. The end of the fourth peak was seen also by the XRT at the beginning of its observations. The XRT detected another flare around 180 s followed by a rapid decay of the light curve by three orders of magnitude before it was overtaken by a plateau at 530 ± 25 s, which lasted for ~ 0.5 day before it bent into a power-law decline. During the fast decline of the prompt emission, the X-ray spectrum changed dramatically from a hard spectrum to a very soft one. After this phase the unabsorbed spectrum of the X-ray afterglow hardened to a power-law with $\beta_X \approx 1.1$ and remained unchanged during the plateau phase and the late power-law decline. The complete light curve obtained from the observations with the BAT (extrapolated to the XRT band), the XRT and XMM-Newton is shown in Fig. 1a; a magnified view of the early times light curve is shown in Fig. 1b.

GRB 060729. *Interpretation:* The CB-model fit to the complete X-ray light curve of GRB 060729 is shown in Fig. 1a. The overall good agreement between theory and observations extends over some eight orders of magnitude in time and in flux. The spectral evolution of the X-ray emission is also in good agreement with the CB-model predictions (see DDD2008b). In the XRT 0.3 -10 keV band the spectrum of the early time flares and their spectral evolution are well described by the exponential cut-off power-law obtained by ICS of a thin thermal bremsstrahlung spectrum, Eq. (12). In particular the exponential factor in Eq. (12) describes well the rapid softening of the spectrum as a function of time during the fast decaying phase of the burst (DDD2008b). But, as soon as the X-ray afterglow is taken over by the synchrotron

emission around 325 s its unabsorbed spectrum changes to the much harder SR power-law spectrum with $\beta_X = 1.1$. The temporal shape of the AG is best fit with electron spectral index $p = 2.20$, which implies $\beta_X = 1.1$, in good agreement with the observations of the XRT and of XMM-Newton (Grupe et al. 2007). The late power law decay satisfies the CB model prediction, $\alpha = \Gamma - 1/2$.

GRB 060729. *Optical observations and a sketch of their interpretation:* The ROTSE-IIIa telescope in Australia took a first 5-s image of this GRB, starting about a minute after the burst, which showed no afterglow down to magnitude 16.6. Some 23 s later, an AG of magnitude 15.7 was clearly detected. The AG brightened over several minutes, and faded very slowly (Quimby et al. 2006b). In the CB model such a behaviour is expected from the early synchrotron emission in the *UVOIR* band during and shortly after the prompt GRB, see Eq. (33). The UVOT followed the *UVO* emission from 739 s to 20 days after trigger. The VLT in Chile obtained spectra, and determined a relatively low redshift of $z = 0.54$ for this burst (Thöne et al. 2006). The light curves of its *UVO* AG show a striking similarity to the X-ray light curve (Grupe et al. 2007) as predicted by the CB model for the optical AG when the bending frequency is below the *UVO* bands, and the extinction along the lines of sight to the hyperluminal CBs stays constant. All in all, the well sampled observations of the *XUVO* light curves of GRB 060729 agree well with the expectations of the CB model.

GRB 061121. *Observations.* This canonical GRB at $z = 1.314$ was described and discussed in detail in Page et al. (2007). It is one of the brightest GRBs in X-rays observed to date by the XRT. The BAT triggered on a precursor to the main burst, allowing observations of the latter from the optical to γ -ray bands. Many telescopes, including Konus-Wind, XMM-Newton, ROTSE, and the Faulkes Telescope North, also observed the burst. Its most intense activity began 60 s after trigger, and consisted of three overlapping peaks of increasing brightness, some 63, 69 and 74 s after trigger, as one can see in Fig. 1d. The γ -ray emission decayed fast after 75 s and became undetectable by the BAT beyond 140 s. The burst was also detected by Konus-Wind. The spectrum and its evolution were well fit with a broken power-law. Its ‘peak’ energy appeared to increase during the rise of each flare and decreased as their flux decayed. But its isolated main strong flare at ~ 74 s, as in many cases studied before, had a maximum E_p at its beginning, which decayed monotonically thereafter. After the bright burst, the X-ray emission —measured by the XRT and later also with XMM-Newton— began to follow the ‘canonical’ decay. Superimposed on the initially rapid decay from the major flare are two smaller flares around 90 s and 125 s. The rapid decay is taken over by the plateau around 200 s and gradually breaks into a power-law decline, with an asymptotic power-law index $\alpha = 1.59^{+0.09}_{-0.04}$. The AG spectrum was well fit by an absorbed power-law with $\Gamma = 2.07 \pm 0.06$, which slightly hardened after the AG bent down.

GRB 061121. *Interpretation:* The hard mean spectral index, $\Gamma \sim 1.3$, and the continuously decreasing E_p during the main flare are as predicted by the CB model (DD2004). The apparent increase of E_p during the rise time of the smaller flares is probably an artifact of overlapping peaks, wherein the decay of a previous flare is taken over by a new flare only near its peak time. A comparison between the observed complete X-ray light curve (Page et al. 2007) and the CB model’s fit is shown in Fig. 1c. The general trend before the onset of the synchrotron plateau is dominated by the main X-ray peak. The two smaller overlapping preceding peaks seen in the γ -ray light curve in Fig. 1d have been included in the fit, and so have the two late X-ray flares not intense enough to be seen in γ -rays. Assuming a constant density ISM, the CB model reproduces very well the observed light curve over seven orders of magnitude in intensity and five in time. The model’s best fit to the entire X-ray light curve yielded $p = 2.2$, which implies $\beta = 1.1$ and $\alpha = 1.6$, in good agreement with their observed values. The CB model also correctly predicts the spectrum and spectral evolution of the X-ray emission during the rapid-decline phase of the prompt emission (DDD2008a). The observed strong softening of the spectrum during the rapid decline is in full agreement with the spectral evolution predicted by Eq. (12). When the plateau phase takes over, the spectral power-law index changes to $\beta_X = 1.07 \pm 0.06$, remaining in agreement with the predicted $\beta = p/2$. The slight hardening of the spectrum at late time to $\beta = 0.87 \pm 0.08$ we have not predicted. It may be an artifact due to the assumption that the absorbing column density is constant during the AG phase.

GRB 061121. *Optical observations and a sketch of their interpretation:* The UVOT detected an optical counterpart in the white filter starting 62 s after the trigger, and subsequently in all other filters (optical and UV). The UVOT light curve shows a prominent peak around $t \sim 73$ s, coincident in time with the blended three main X-ray peaks, followed by a plateau phase. The complete optical light curves measured by the Swift UVOT and in ground observations with ROTSE, FTN, CTIO and MDM follows roughly the canonical X-ray light curve. The peak is well fit by SR from expanding CBs in a windy density $\propto 1/r^2$. The rest of the light curve, as the canonical X-ray light curve, is well described by SR from a CB decelerating in a constant density with a spectral index gradually changing from $\beta \sim 0.5$ above the bend frequency to $\beta = \beta_X \sim 1$ below it, well after the AG bends down.

GRB 050315. *Observations:* This GRB was described and studied in detail by Vaughan et al. (2006). It is one of the first Swift GRBs with a well sampled X-ray light curve from trigger until late time (~ 10 days). It was detected and located by BAT at 20:59:42 UT on March 15, 2005. The BAT light curve comprises two major overlapping peaks separated by about 22 seconds. Absorption features in the spectrum of its optical afterglow obtained with the Magellan telescope indicated that its redshift is $z \geq 1.949$ (Berger et al. 2006). The XRT began observations 80 s after the BAT trigger and continued them for 10 days, providing one

of the best sampled X-ray AGs (Vaughan et al. 2006). The extrapolation of the BAT light curve into the XRT band-pass showed the X-ray data to be consistent with the tail end of the decaying prompt emission. The combined light curve showed the canonical behaviour: the rapid decline ends ~ 300 s after trigger, the plateau lasted for about 10^4 seconds, before it gradually bent into a power-law decay.

GRB 050315. *Interpretation:* The complete X-ray light curve of this GRB is compared with the CB-model prediction in Fig. 1e. An enlarged view at early times is shown in Fig. 1f. Two pulses are used in the fit. As shown, the model reproduces the data well: the exponentially decaying contributions of the two pulses describe the changing slope of the fast-decaying phase. The early ICS flares, the decay of the prompt emission and the subsequent synchrotron-dominated plateau and gradually bending light curve into a power-law decay are well reproduced by the model as shown in Figs. 1e,f.

5.1.2. GRBs with a single power-law afterglow

GRB 061007. *Broad-band observations:* The data were summarized and discussed by Mundell et al. (2007) and Schady et al. (2007). The Swift BAT detected the event on 2006 Oct 07, 10:08:08 UT. The prompt emission was also detected at MeV energies by Konus-Wind, Suzaku-WAM and RHESSI. The BAT γ -ray light curve has three peaks with substantial sub-structure, and a small fourth peak around 75 s that shows a long exponential decay and a faint emission detectable till ~ 900 s. The Swift XRT and UVOT began observing 80 s after the BAT trigger time and detected a very bright X-ray and optical counterpart with a power-law decay identical to that of the soft γ -ray tail, with a temporal slope $\alpha_X = 1.6 \pm 0.1$ all the way to at least 10^6 s with no indication of any break. The best-fit spectral index of the unabsorbed X-ray afterglow was $\Gamma = 2.1 \pm 0.1$. Robotically-triggered observations with the ground-based telescopes ROTSE and FTS began at 26 s and 137 s after trigger, respectively, and the FTN continued them for 5.5 h. Follow-up observations were performed with the VLT and the Magellan-I Baade telescope. The spectral indices of the unabsorbed X-ray and unextinct optical AGs were found to be the same beyond 200 s.

GRB 061007. *Interpretation:* In the CB model, afterglows decaying like a single power-law are observed when the AG's bend takes place very early and is hidden under the prompt emission, or before the beginning of the observations. In the case of a constant ISM density, the decay index and the spectral index are predicted to satisfy $\alpha = \Gamma - 1/2$ implying a decay index $\alpha = 1.6 \pm 0.1$. The CB-model predictions for the light curves of the X-ray and R -band AG are shown in Figs. 2a,b. The best-fit temporal decay index is 1.6, as expected. Agreement between theory and observations is very good. The slight wiggling around the power-law

decay follows, in the CB model, from density variations along the trajectory of the CBs. The reported broad-band spectral index, corrected for extinction and absorption, is $\beta_{OX} = 1.03$. (Mundell et al. 2007). This is consistent with the CB-model’s prediction (DDD2002) for a bend frequency below the optical band, as expected beyond the AG’s break.

GRB 061126. *X-ray observations:* The broad-band observations of this GRB were described and discussed in detail in the framework of the fireball model by Perley et al. (2008) who found their evolution troublesome and by Gomboc et al. (2008) who found them intriguing. It was a long GRB ($T_{90} = 191$ s) dominated by two major γ -ray peaks within the first 40 s, which was followed by a smooth power-law decline with a temporal index $\alpha \sim 1.3$. Due to an Earth limb constraint Swift slewed to the burst only after 23 min and followed its X-ray AG from 26 min to 20 days after burst. Its X-ray AG showed roughly a power-law decline with the same power-law index, $\alpha_X \sim 1.3$, with marginal evidence for steeper early and very late time-declines, with an index $\alpha \sim 2$. The unabsorbed X-ray AG had a best-fit spectral index $\beta_X = 0.94 \pm 0.05$.

GRB 061126. *Optical observations:* In the optical band this was one of the brightest Swift GRBs. Its optical emission was detected by RAPTOR during the γ -ray emission 21 s after the BAT trigger, and its early decline was followed also by the PAIRITEL, NMSU, KAIT, Super Lotis and FTN robotic telescopes. Observations continued with several large telescopes. The data were summarized and discussed in Perley et al. (2008) and in Gomboc et al. (2008). The initial power-law decay of the optical AG with $\alpha \sim 1.5$ changed to a shallower decline approximately 1000 s after the burst, which steepened about 1.5 d after the burst. The last optical data point ($0.52 \pm 0.05 \mu\text{Jy}$) obtained with Gemini North at 15 d after burst (Gomboc et al. 2008) was slightly dimmer than the host galaxy at redshift $z = 1.16$ (Perley et al. 2008), whose R -magnitude 24.10 ± 0.11 ($0.70 \pm 0.07 \mu\text{Jy}$) was measured with the Keck telescope 54 d after burst. After correcting for Galactic extinction and estimated extinction in the host galaxy, its observed early-time optical emission had $\beta = 1.0 \pm 0.1$ and showed a strong colour evolution towards $\beta_O \sim 0.4 - 0.5$ around 2000 s. The late-time index was typically $\beta_O = 0.95 \pm 0.10$, consistent with $\beta_O = \beta_X$.

GRB 061126. *Interpretation:* Swift’s XRT detected the X-ray emission only long after the prompt signal had faded. Its measured light curve, shown in Fig. 2c, was well fit by SR, with $p = 1.84$, in a density $n \propto 1/r^2$, taken over by a constant at $t \sim 3000$ s. The CB-model expectation, $\Gamma = p/2 + 1 = 1.92$, is consistent with the mean photon spectral index (corrected for absorption), inferred by Evans et al. (2007), $\Gamma = 1.82 \pm 0.05$, and by Perley et al. (2008), $\Gamma = 2.00 \pm 0.07$. The wiggling around the power-law decay –induced by density variations along the CB’s path– we did not model. In the FB model prompt and AG emissions are SR-dominated and the extrapolation from the γ - and X-domains to the optical band results

in a signal much brighter and with a different light curve than the observed one (Perley et al. 2008). The changing power law of the declining optical light is well described by SR from a CB with the same parameters modeling the X-ray light curve. A SN contribution akin to that of SN1998bw placed at the GRB location was added to the CB light curve. The general behavior is well reproduced by the CB model, as can be seen from Fig. 2d. The slight wiggling of the light curve around its CB model’s description and the corresponding changes in the spectral index β_O we attribute, as usual, to small density variations, which we did not model. The expected variation of the spectral index from $\beta_O \approx 0.5$ at early time to $\beta_O \approx \beta_X$ is supported by the data (Perley et al. 2008). The evolution of $\beta_O(t)$ at very early time may be due to variation in light extinction as the CB moves away from the SN.

GRB 080319B *Observations:* This GRB was detected by the Swift (Racusin et al. 2008b), INTEGRAL (Beckmann et al. 2008) and Konus-Wind (Golenetskii et al. 2008) satellites. It lasted ~ 60 s. It was the brightest observed long GRB so far. Three robotic ground telescopes detected its extremely intensive optical light emission (Karpov et al. 2008, Cwiok et al. 2008, Wozniak et al. 2008) before the Swift alert, and saw it brightening to a visual peak magnitude 5.4, visible to the naked eye, some 18 s after the start of the burst. Swift XRT slewed to the GRB position within 65 s and followed its power-law declining X-ray light curve for the first 15 days. Swift’s prompt alert sent to the world’s telescopes triggered many follow-up observations including spectral measurements with the VLT (Vreeswijk, et al. 2008) and Hobby-Eberly telescope (Cucchiara et al. 2008) which determined the GRB’s redshift to be $z = 0.937$. Its X-ray light curve is shown in Fig. 2e. Its combined R - and V -band light curve (normalized to the R -band), as reported in GCNs (see, e.g., Bloom et al. 2008 and references therein) is shown in Fig. 2f.

GRB 080319B. *Interpretation:* In the CB model the ICS spectrum of the scattered glory’s photons is an exponential cut-off power-law with a spectral index, $\Gamma \approx 1$, cut-off energy $\approx E_p$, and a power-law tail, see Eq. (4). The spectral index, $\Gamma = 1.01 \pm 0.02$ in the 15 -350 keV range, reported by the Swift BAT team (Racusin et al. 2008b), and the Band function fit to the broader 20 keV to 7 MeV energy range, reported by the Konus-Wind team (Golenetskii et al. 2008) are in agreement with the CB model.

In Fig. 2e we compare the X-ray light curve of GRB 080319B, measured with the Swift XRT, to its CB-model description, Eq. (26), assuming a constant ISM density and a single effective CB. The best-fit p is 2.08, yielding an approximate power-law decline with $\alpha_X = 1.54$ beyond t_b , best fit to 72 s. The description of the AG is quite good except around 4×10^4 s, where the data are sparse. As expected (DDD2008a) for very luminous GRBs, no AG break is observed. The temporal index, $\alpha_X = \Gamma_X - 1/2 = 1.42 \pm 0.07$, predicted from the late-time photon spectral index, $\Gamma_X = 1.92 \pm 0.07$, reported by the Swift XRT team (Racusin et

al. 2008c) is in agreement with the best-fit temporal index. At $t \sim 4 \times 10^4$ s, the data lie below the fit. If not a statistical fluctuation, this may be due to a failure of the constant-density approximation, not surprising at this level of precision.

GRB 080319B began with a succession of prompt γ -ray pulses, but the XRT observations started too late to detect their X-ray counterparts, which were seen at optical frequencies. Even though the optical pulses are SR-generated, their expected time dependence, Eq. (33), is akin to that of the γ -ray pulses. The CB-model optical light curve, shown in Fig. 2f, was obtained by fitting each of the three early pulses observed by TORTORA (Karpov et al. 2008). The later-time AG, described by Eq. (26) for $t_b \gtrsim 70$ s, is essentially a power-law decline, insensitive to the precise values of the best-fit $\theta \gamma_0$ and t_b , but sensitive to β_O . In the CB model, the index β is ~ 0.5 below and ~ 1.1 above the bend frequency, which usually crosses the optical band within $t \sim 1$ day, so that $\beta_O \approx \beta_X$ thereafter. Our best fit to the optical AG results in $\alpha_O = 1.40 \pm 0.04$, which implies a late-time $\beta_O \approx 0.90$, consistent with the expectation. So far no late-time spectral information is available to verify it.

When a CB crosses a density enhancement, ν_b increases due the sudden increase in n and the consequently faster CB deceleration. The bend frequency may then cross the optical band ‘backwards’: from above it, to below it. Such a spectral evolution may have been observed some 5000 s after the onset of the burst (Bloom et al. 2008). The spectral analysis of the UNLV GRB group (Zhang et al. 2008) shows a decreased $\beta_X = 0.70 \pm 0.05$ around that time. The expected $\beta_O \approx \beta_X - 0.5 = 0.2 \pm 0.05$ at that time is consistent with the spectral evolution around 5000 s after burst reported by Bloom et al. (2008).

5.1.3. GRBs with a semi-canonical X-ray light curve

GRBs 060211A, 061110A, 080307, 051021B, 080303, 070220. *Observations and interpretation:* These GRBs, detected by the Swift BAT and followed up by its XRT, have canonical X-ray light curves, but for the fact that their exponentially-declining phase at the end of the prompt emission changed into a slower power-law decline before it entered the plateau phase. Their X-ray light curves and their CB-model description are shown in Figs. 3a-f. The exponential decline of the prompt ICS emission, as given by Eq. (12), is taken over by the SR emission from the CBs, which, in a windy circumburst environment, decays like a power: $F_\nu \sim t^{-(1+\beta_X)} \nu^{-\beta_X}$, see Eq. (33). This takeover by SR is accompanied by a sudden hardening of the AG to the ordinary SR spectrum, $\sim \nu^{-\beta_X}$ with $\beta_X \sim 1.1$. The power-law decay changes into the canonical plateau when the CBs enter the constant ISM density. In the case of GRB 070220, the fast asymptotic decline was well fit assuming an isothermal sphere density profile, $n \propto 1/(r^2 + r_c^2)$, as in the cases shown in Figs. 6,7.

5.1.4. *GRBs with large X-ray flares during the early X-ray afterglow*

GRB 060526. *X-ray observations:* This GRB was detected by Swift’s BAT at 16:28:30 UT on May 26, 2006 (Campana et al. 2006a). The XRT began observing the field 73 s after the BAT trigger. The burst started with a γ -ray emission episode lasting 18 s. The GRB was thereafter quiet for about 200 s, and then emitted two additional pulses which lasted about 50 s and were coincident with strong X-ray flares between 220 s and 270 s after trigger. The XRT followed the X-ray emission for 6 days until it faded into the background. The entire XRT light curve is shown in Fig. 4a. It has the canonical behaviour of many Swift GRBs, and two superimposed early-time large flares.

GRB 060526. *Optical observations:* The observations of the optical emission from GRB 060526 are summarized and discussed in Dai et al. (2007), Khamitov et al. (2006) and Thöne et al. (2008b). They were started as early as 36.2 s after the BAT trigger by the Watcher 40cm robotic telescope, in South Africa, which saw the AG at a very bright 15th magnitude (French & Jelinek 2006). The UVOT on Swift detected its optical AG 81 s after trigger (Campana et al. 2006a). The burst was followed up with UVOT and ground-based telescopes by several groups. Spectra obtained with the Magellan-Clay telescope indicated a redshift of $z = 3.21$ (Berger & Gladders 2006). Its R -band light curve obtained with the MDM and PROMPT telescopes at Cerro Tololo, amongst others, is shown in Fig. 4c (Dai et al. 2007 and references therein). It can be seen in Figs. 4a,b that, apart from the superimposed large early-time X-ray flares which are not present in the optical light curve and the late mini-flares, the X-ray light curve and the well-sampled R -band data show a roughly achromatic behaviour.

GRB 060526. *Interpretation:* The entire X-ray light curve and its CB-model’s fit are shown in Fig. 4a. Three ICS pulses were used in the fits of the early time emission, although the third pulse may well be a superposition of two unresolved ones. The pulse shape and the spectral evolution of the last two large flares are typical of ICS flares (DDD2008a). Their coincidence in time with the late γ -ray peaks, the absence of corresponding peaks in the optical UVOT light curve, and their spectral evolution support their interpretation as part of the prompt GRB emission. This GRB’s ‘prompt’ emission extends to long times partly because of the large redshift of the burst source which stretches observer time by the relatively large factor, $z + 1 = 4.21$. A zoom-in on these two ICS X-ray flares is shown in Fig. 4b. The decay of the prompt emission is dominated by the decay of the last pulse. In Figs. 4a,b,c we show that the early ICS flares, the decay of the prompt emission, the subsequent synchrotron-dominated plateau and the gradual bending into a power-law decline are all well reproduced by the CB model. In Fig. 4d we show the theoretical R -band light curve obtained with the parameters which were fitted to the SR X-rays. Since the bending frequency during the steepening phase

is below the R band, the temporal decay of the R -band light curve practically coincides with that of the X-ray one. Both the X-ray and the late-time optical light curve are bumpy, which may be caused by mini-flares and/or density inhomogeneities, which we have not tried to fit. The apparent steeper decay of the optical AG beyond 1 day may be the decline following a flare or a transition into the galactic halo with a density declining as $1/r^2$.

GRB 060206. *Observations:* This GRB triggered the Swift’s BAT on February 6, 2006 at 04:46:53 UT (Morris et al. 2006). Its γ -ray emission lasted only 6 s. The XRT started its observations 80 s after the BAT trigger. Despite its initially poor time sampling, it detected an X-ray decline after 0.5 h and a strong rebrightening after 1 h, after which its follow-up was nearly continuous for some 20 days. The bright optical AG of GRB was detected by Swift at $V = 16.7$, about 1 minute after the burst. RAPTOR started observations 48.1 min after trigger and reported that, after an initial fading, the AG rebrightened 1h after burst by ~ 1 magnitude within a couple of minutes (Wozniak et al. 2006). Many observatories followed the bright optical AG (Monfardini et al. 2006, Stanek et al. 2007, and references therein), and Fynbo et al. (2006a) carried out spectral observations to determine its large redshift, $z = 4.05$, later confirmed by other groups. The RAPTOR data clearly shows that the rebrightening was due to two flares (Wozniak et al. 2006). Similar ‘anomalous’ rebrightennings of the optical AG were seen in some other bursts (Stanek et al. 2007) .

GRB 060206. *Interpretation:* In Fig. 4a,b we compare the observations of the X-ray and R -band light curves with the CB-model fits. Superimposed on the plateau phase are two strong flares beginning around 1 h after trigger. The coincidence in time of the X-ray and optical flares, and the absence of any evidence for the typical ICS strong spectral evolution, suggest that these two flares are SR flares due to an encounter with a density jump, such as at the boundary of a superbubble created by the star formation region. In Fig. 4c we compare the observed light curve of these two flares in the R band and their CB-model description via Eq. (33). The figures show that the agreement is very good and that there is nothing ‘anomalous’ in the X-ray and optical data of GRB 060206. Instead, their prominent structures are well described and precisely related by their CB-model’s understanding in terms of SR from late ejections of CBs into the circumburst windy environment.

5.1.5. GRBs with chromatic afterglows

GRB 050820A. *Broad-band observations:* This is one of the Swift GRBs with the best-sampled broad-band data, summarized and discussed in detail in Cenko et al. 2006. The burst was detected and observed by Swift and Konus-Wind. Its γ -ray emission was preceded by a soft precursor pulse some 200 s before the main burst. The latter lasted some 350 s and

consisted of 5 well-separated major peaks, with a clear spectral-softening evolution within each peak. The main peak observed by Swift during $217\text{ s} < t < 241\text{ s}$, and the time-integrated photon spectrum over the entire burst were well fit with a cut-off power law with a photon indices $\Gamma = 1.07 \pm 0.06$ and $\Gamma = 1.12 \pm 0.15$, respectively. The Swift XRT began observations 88 s after trigger and followed its X-ray emission until 44 days, see Fig. 5a. The measured mean photon index of the unabsorbed emission in the 0.3-15 keV band during the prompt emission phase was $\Gamma = 1.06 \pm 0.04$ ($\beta_X = 0.06 \pm 0.04$) and $\Gamma = 2.06 \pm 0.07$ ($\beta_X = 1.06 \pm 0.07$) during the afterglow phase (Evans et al. 2007).

The prompt optical emission was measured by RAPTOR beginning 18 s after trigger. The Swift UVOT began observations 80 s after trigger but became inoperable when Swift entered the South Atlantic Anomaly approximately 240 s after trigger. The automated Palomar 60-inch telescope started observations 206 s after trigger and followed-up until late time. Later measurements were made by the Turkish Russian 1.5 m telescope. Late-time images were taken with the 9.2 m Hobby-Eberly Telescope and with the Hubble Space Telescope until 37 days after burst. The *R*-band light curve is shown in Fig. 5b. Ignoring host reddening and correcting for Galactic extinction in the burst direction [$E(B-V) = 0.044$], the fitted spectral index (Cenko et al. 2006) in the optical band during the prompt emission was $\beta_O = 0.57 \pm 0.06$, steepening to $\beta_O = 0.77 \pm 0.08$ within the first day. While the optical spectrum appeared steeper later on, the poor fit quality precluded the derivation of a reliable value. In Figs. 5a,b one can see the very chromatic behaviour of the X-ray- and optical light curves during the prompt and AG phases.

GRB 050820A. *Interpretation:* The pulse shape of the prompt-emission γ /X-ray peaks and their spectral index agree well with those predicted by ICS of glory light. The CB-model fit to the entire XRT light curve is shown in Fig. 5a. The early-time light curve is well described by the ICS X-ray counterparts of the prompt γ -ray peaks: the very-early-time XRT light curve is the tail of the precursor pulse, the next pulse is the X-ray counterpart of the first ICS γ -ray pulse around 220 s. The ICS peaks are superimposed on a canonical SR afterglow bending down at around 1000 s. We interpret the X-ray peak around 5000 s as a flare due to a density bump. While the prompt γ -ray and X-ray emission is dominated by the ICS of glory light, which yields $\beta \sim 0$, the optical emission is dominated by SR, as in Eq. (33), with the typical $\beta \sim 0.5$, as observed. The different radiation mechanisms are responsible for the chromatic behaviour of the prompt emission.

Although both the X-ray AG and the optical AG are dominated by SR, the optical AG evolves differently than the X-ray AG because of its dependence on the bend frequency, a function of the ISM density and the Lorentz factor of the decelerating CB. Consequently, the early-time optical and X-ray AGs are chromatic until the bend frequency crosses well

below the optical band, after which $\beta_O = \beta_X$. This is shown in Figs. 5a,b. The CB-model R -band light curve in Fig. 5b was calculated with $\beta_O = 0.77$ and the best-fit parameters of the X-ray AG shown in Fig. 5a. The calculated light curves did not include the late-time flares in order not to obscure the chromatic behaviour of the underlying smooth AGs.

GRB 060418. *Broad-band observations:* This GRB was discussed in detail in Molinari et al. (2007). Its γ -ray emission was detected and observed by the Swift BAT and by Konus-Wind. The BAT light curve showed three overlapping peaks at 10, 18 and 27 s and a bump which coincided with an X-ray flare at 128 s after trigger. The Swift XRT started observing the GRB 78 s after trigger. The XRT light curve shows a notable flaring activity superimposed on a smooth AG decay. A prominent peak, also visible as a bump in the BAT data, was observed at about 128 s after trigger. The REM robotic telescope began observing this GRB 64 s after trigger in the $z'JHK$ bands and followed it down to the sensitivity limits. The *UVONIR* AG was also detected by the Swift UVOT, by one of the 16-inch PROMPT telescopes at CTIO and by the robotic telescope FRAM (part of the Pierre Auger Observatory). The *ONIR* AG was also followed up with the 1.3 m telescope at CTIO beginning ~ 1 h post-trigger, and with the PAIRITEL 1.3 m telescope staring 2.53 h after trigger. The *UVONIR* light curves show a very chromatic initial behaviour compared to the XRT light curve, see Figs. 5c,d. The *NIR* AG rises until reaching a maximum around 130 s after trigger and then gradually changes to a power-law decline shallower than that of the X-ray AG, with a weak flare superimposed on it at around 5 ks, which roughly coincides in time with a strong X-ray flaring activity.

GRB 060418. *Interpretation:* The XRT light curve was fit by the tail of the prompt ICS emission, and an ICS flare around 128 s which was later taken over by the SR afterglow of a CB moving in a constant density ISM (Fig. 5c). The bend of the SR afterglow is hidden under the tail of the X-ray flare at 128 s. The H -band light curve, shown in Fig. 5d, was calculated using Eq. (33) with an early-time unabsorbed $\beta_O = 0.5$ and an ejection time, $t_i = 26$ s, coincident with the start-time of the major γ -ray peak. No attempt was made to model the flaring activity around 5 ks.

GRB 071010A. *Broad-band observations:* This GRB at redshift $z = 0.985$ was discussed in detail by Covino et al. (2008). It had a single peak lasting for 6 s, detected by the Swift BAT. Swift did not slew to this GRB because its automatic slewing was temporarily disabled. The XRT began observing this GRB only 34 ks after the BAT trigger and followed it until 550 ks after trigger. The XRT light curve (Fig. 5e) shows a wide flare peaking around 60 ks and followed by a power-law decay with an index $\sim 1.6 \pm 0.3$. The early *ONIR* emission was observed by the TAROT, REM and the 2.2 m MPI-ESO telescopes. Follow-up *NIR* observations were carried out with Gemini-North, TNG and the NTT. The AG was observed

a few hours after the GRB with the Keck-I and Sampurnan telescopes and with NOT and VLT. The *ONIR* light curve shows an initial rising with a maximum at about 7 min, and a smooth decay interrupted by a flare about 0.6 d, visible in both the *ONIR* and in X-rays (Figs. 5e,f). The *ONIR* spectrum was modeled by a power law with an SMC-like extinction law with a best fit $E(B-V) = 0.21$. The reported unabsorbed late index was $\beta_O = 1.26 \pm 0.26$.

GRB 071010A. *Interpretation:* The *ONIR* light curves correspond to the SR radiation from a CB ejected into a windy $1/r^2$ density profile, as given by Eq. (33), until taken over by a constant-density ISM, with a standard wide flare superimposed on the AG around 0.6 d. The late XRT light curve was calculated with the same parameters except for $\beta_X = 1.1$.

5.1.6. GRBs with very fast-decaying late afterglows

In Figs. 6 and 7 we show the well-sampled XRT light curves of 12 GRBs: 050318, 050326, 050814, 051008, 061019, 060807, 060813, 070306, 070419B, 070420, 070521 and 080207, with a late decay more rapid than the canonical $t^{-1.6}$ decline of the AG of CBs decelerating in a constant-density ISM. In the CB model such a fast decline is produced by a fast-declining ISM density or by the tail of a late flare. We have found that all Swift GRBs with a well sampled fast-declining X-ray light curve can be reproduced by either an asymptotic $n \propto 1/r^2$ density profile or a tail of a late flare, as demonstrated in Figs. 6 and 7. Such an asymptotic density decline is typical of isothermal spheres, for which $n(r) \sim n_0/[1+(r/r_c)^2]$, a fair representation of the density profile of galactic bulges in spirals, of ellipticals, and of the outskirts of bumpy density shells created by stellar winds. The CB-model prediction is that for $r \gg r_c$, the AG declines like $F_\nu \propto t^{-(1+\beta)} \nu^{-\beta}$, i.e. with $\alpha = \beta + 1 = \Gamma_{SR} \sim 2.1$. In some GRBs the transition from $\alpha = \Gamma - 1/2 \sim 1.6$ for $r \ll r_c$, to $\alpha = \Gamma \sim 2.1$ for $r \gg r_c$, has probably been misidentified as the standard FB-model late achromatic ‘jet break’ (e.g. Dai et al. 2008, Racusin et al. 2008a).

5.1.7. GRBs with complex chromatic light curves

GRB 050319. *Observations:* The Swift BAT, XRT and UVOT observations of this GRB were discussed in detail in Cusumano et al. (2006a) and Mason et al. (2006). A reanalysis of the BAT data showed that its onset was ~ 135 s before the trigger time reported by Krimm et al. (2005). The XRT began its observations 90 s after the BAT trigger, continuing them for 28 days (Cusumano et al. 2006a). The γ -ray light curve shows two strong peaks. The X-ray light curve had the canonical behaviour: an early fast decline which extrapolated well

to the low-energy tail of the last prompt γ -ray pulse at around 137 s after the onset of the GRB. After ~ 400 s, the fast decline was overtaken by a plateau which gradually bent into a power-law decline after $\sim 10^4$ s.

GRB 050319. *Interpretation:* A CB-model fit to the complete X-ray light curve is shown in Fig. 8a. Two pulses are used in the early ICS phase. The early ICS flares, the decay of the prompt emission and the subsequent synchrotron-dominated plateau and gradually bending light curve are well reproduced. The spectral index of the AG, $\beta_X = 0.73 \pm 0.05$, and its asymptotic temporal decline index, $\alpha = 1.14 \pm 0.2$ (Cusumano et al. 2006a), satisfy well the relation $\alpha = \beta + 1/2$, though they were obtained by correcting only for Galactic absorption.

GRB 050319. *UVO observations:* The UVOT detected an optical counterpart in the initial White filter observation, starting 62 s after the trigger, and subsequently in all other filters (optical and UV). Swift’s UVOT, which followed the typical sequence for GRB observations, was able to observe the UVO emission 140 s after its detection by the BAT. It was also observed by ground-based telescopes RAPTOR (Wozniak et al. 2005), and ROTSE III (Quimby et al. 2006a) just 27.1 s after the Swift trigger. The optical AG was followed later with a number of ground-based telescopes (Huang et al. 2006 and references therein). An absorption redshift, $z = 3.24$, was measured with the Nordic Optical Telescope (Jakobsson et al. 2006). The afterglow of this GRB is highly chromatic with no apparent correlated behaviour between its X-ray and optical emission, as can be seen from Figs. 8a,b.

GRB 050319. *Interpretation of UVO observations:* The early-time optical light curve was fit by SR emission from the two separate CBs implied by the first two strong γ -ray peaks. The late X-ray and optical AG were calculated with the same deceleration parameters. The complex optical light curve is reproduced well, as shown in Fig. 8b.

GRB 060605. *Broad-band observations:* This GRB at $z = 3.773$ was studied and discussed by Ferrero et al. (2008). It was long and relatively faint, with a duration of about 20 s, detected by the Swift BAT. The BAT light curve showed two overlapping peaks. The Swift XRT began taking data 93 s after the BAT trigger and continued for 200 ks. The XRT light curve shows a canonical behaviour with a flare around 265 s after trigger, superimposed on a shallow plateau which began at ~ 200 s and changed into an asymptotic power-law decline beyond 8 ks (Fig. 8c). The best-fit spectral index of the unabsorbed spectrum in the X-ray band was $\beta_X = 1.06 \pm 0.16$. The UVOT, which began observations of the GRB’s field 97 s after trigger detected and localized its fading AG. Follow-up observations in the *UVONIR* bands were carried out also with ROTSEIIIa, which began 48 s after trigger and with the VATT, RTT, TNG and the Kitt Peak 2.1 m telescopes. In Fig. 8d we show the recalibrated R_c -band light curve from these observations (Ferrero et al. 2008). In contrast with the XRT light curve, it shows a chromatic early rise with a ‘broken’ power-law decay.

The *XUVONIR* data show a spectral evolution at early time from $\beta_{OX} = 0.8 \pm 0.05$ at 0.07 d, to $\beta_{OX} = 1.02 \pm 0.02 \approx \beta_X$ at 0.43 d.

GRB 060605. *Interpretation:* The XRT light curve was fitted with a canonical CB-model X-ray light curve (Fig. 8c), beginning with the tail of the fast decline of the prompt ICS emission, and taken over by SR in a constant density environment which changes to an $1/r^2$ profile beyond 8 ks. The bump around 250 s was interpreted as a SR flare superimposed on the smooth canonical AG. The corresponding *R*-band light curve, shown in Fig. 8d, was generated using Eq. (33) with the fit parameters of the X-ray flare and the canonical $\beta_O = 0.5$ for an early optical emission, until it was taken by the SR emission in the density profile used in the CB-model description of the late X-ray AG.

GRB 060607A. *Broad-band observations:* This GRB at $z = 3.082$ was studied by Molinari et al. (2007), Nysewander et al. (2007) and Ziaee pour et al. (2008). The Swift XRT began observing it 73.6 s after the BAT trigger. Its complex X-ray light curve, like that of quite a few other GRBs, was dominated by strong flaring activity. The XRT light curve, shown in Fig. 8d, exhibits three early flares peaking at approximately 97 s, 175 s, and 263 s after trigger and a continuing weaker flaring activity superposed on a decaying continuum. The UVOT began to observe the bright optical AG 75 s after trigger. The REM telescope began *NIR* observations 59 s after trigger. It detected a brightening smooth light curve which peaked around ~ 155 s and decayed like a power law interrupted by flaring activity beyond 1000 s. The REM followed the decay for 20 ks down to its sensitivity limit. Four 0.4m PROMPT telescopes began observing the AG 44 s after trigger and measured the *UVO* light curves until 20 ks, which behaved as the *NIR* light curve (Nysewander et al. 2007).

GRB 060607A. *Interpretation:* The complex X-ray light curve, shown in Fig. 8e, was fit with 6 flares superimposed to the AG of a single dominant CB. This fit, which can be improved by splitting the last flare into two, is a very rough description ($\chi^2/dof = 4.9$ for 440 *dof*), not a proof of the quality of a prediction. Moreover, in cases with such a prominent flaring activity, the mean spectral index of the AG data is an average between the typical index of flares, $\Gamma = 1.5$, and that of a SR afterglow, $\Gamma = 2$, i.e. an average significantly smaller than that of the SR. Thus, we do not expect such a labyrinthine AG to satisfy the CB-model spectral-index relations, Eqs. (28,29). The CB model's early *UVONIR* light curves, shown in Fig. 8f for the *H* band, is well described by the smooth SR afterglow of a single CB moving in a wind environment, as given by Eq. (33). We did not try to fit the weak flaring activity, which is probably due to a bumpy environment.

5.1.8. *XRF 060218*

XRF 060218/SN2006aj. *Broad-band observations:* This XRF/SN pair provides one of the best testing grounds of theories (De Rújula 2008) given its proximity, which resulted in very good sampling and statistics (see, e.g. Campana et al. 2006b, Pian et al. 2006, Soderberg et al. 2006, Mirabal et al. 2006, Modjaz et al. 2006, Sollerman et al. 2006, Ferrero et al. 2006, Kocevski et al. 2007). The XRF was detected with the Swift’s BAT on February 18, 2006, at 03:34:30 UT (Cusumano et al. 2006b). The XRT and UVOT detected the XRF and began taking data 152 s after the BAT trigger. Its detection led to a precise localization, the determination of its redshift, $z = 0.033$ (Mirabal et al. 2006) and the discovery of its association with a supernova, SN2006aj (Masetti et al. 2006). The BAT data lasted only 300 s, beginning 159 s after trigger, with most of the emission below 50 keV (Campana et al. 2006b, Liang et al. 2006). The total isotropic equivalent γ -ray energy was $E_{\text{iso}} \sim 0.8 \times 10^{49}$ erg and the spectral peak energy, E_p , strongly evolved with time from ~ 54 keV at the beginning of observations by the BAT down to < 5 keV 300 s later. The X-ray light curve was followed up with the XRT until nearly 1.1×10^6 s after burst (Campana et al. 2006b). It showed the canonical behaviour of X-ray light curves of XRFs and GRBs, except that the prompt X-ray emission was stretched in time and lasted more than 2000 s. The prompt emission ended with a fast temporal decline and a rapid spectral softening (Fig. 9a) that was overtaken around 10 ks by an ordinary power-law-decaying AG. Follow-up observations with the UVOT and ground-based telescopes showed a very chromatic *UVONIR* AG with a long brightening phase with a peak between 30 and 60 ks, which changed into a fast decline and was taken over around 2 d after burst by the rising light curve of SN2006aj (Marshall et al. 2006, Campana et al. 2006b, Pian et al. 2006, Mirabal et al. 2006, Sollerman et al. 2006, Ferrero et al. 2006). Spectral measurements of the the light of SN2006aj showed negligible additional extinction (Pian et al. 2006, Guenther et al. 2006, Wiersema et al. 2007) beyond the Galactic one, $E(B - V) = 0.13$, along the line of sight.

XRF060218/SN2006aj. *Interpretation:* The spectral energy distribution measured with the Swift BAT and XRT was parametrized (e.g. Campana et al. 2006b, Liang et al. 2006, Butler et al. 2007) as the sum of a black-body emission with a time-declining temperature from a sphere with time-growing radius, and a cut-off power-law with time-dependent amplitude and a constant cutoff energy. From this parametrization it was concluded that this event had a thermal black-body component in its X-ray spectrum, which cools and shifts into the *UVO* band as time elapses. This alleged black-body component was interpreted as the result of a shock’s break-out from the stellar envelope into the stellar wind of the progenitor star of the core-collapse SN2006aj (Campana et al. 2006b, Blustin 2007, Waxman, Meszaros & Campana 2007). From this interpretation, a delay of ≤ 4 ks between the SN and the GRB beginning was concluded.

The early optical emission from XRF 060218 –the first 10^5 s measured with the UVOT and interpreted as black-body dominated– required an intrinsic reddening of $E(B - V) = 0.20 \pm 0.03$ (assuming a Small Magellanic-Cloud effect) in addition to a Galactic reddening of $E(B - V) = 0.14$ (Campana et al. 2006b, Ghisellini et al. 2007) to be consistent with a black-body spectrum. Such a host extinction is inconsistent with the negligible extra-Galactic one measured from the spectrum of SN2006aj by e.g., Pian et al. (2006), Guenther et al. (2006), Wiersema et al. (2007). With a negligible reddening in the host, the ratio between the measured fluxes with the V and UVW2 filters of the Swift UVOT –de-reddened with the Galactic $E(B - V) = 0.14$ – is different by nearly a factor 10 from the $F_\nu \propto \nu^2$ behaviour in the Rayleigh-Jeans domain. Moreover, the flux ratio between these two bands is time-dependent and increases by ~ 2.5 between 2 ks and 20 ks after burst, while it should be constant as long as the optical band stays in the Rayleigh-Jeans part of the black-body spectrum. We conclude that the *UVO* emission from XRF 060218 is not black-body-like. This is independent of whether it is produced by the same source which produced the alleged black-body component in the prompt X-ray and γ -ray emission or by another source.

The light curves of XRF 060218/SN2006aj, measured with the Swift’s UVOT filters, are particularly interesting. Not only they provide evidence that the XRF was produced in the explosion of SN2006aj, but, together with the BAT and XRT light curves, they confirm the CB-model interpretation of the broad-band emission at all times. Prior to the dominance of the associated supernova’s radiation, the *UVO* light curves show wide peaks whose peak-time shifts from $t_{peak} \approx 30$ ks at $\lambda \sim 188$ nm to $t_{peak} \approx 50$ ks at $\lambda \sim 544$ nm, and whose peak-energy flux decreases with energy, see Fig. 9b: the lower half of the upper figure. In the CB model these are the predicted properties of a single peak generated by a single CB as it Compton up-scatters glory’s light. The prompt γ -rays and X-rays of ordinary GRBs are dominated by ICS, while the optical emission is dominated by SR. However, in low-luminosity XRFs the optical emission is also dominated by ICS of glory light. The dominant radiation mechanisms at various times can actually be identified, using the different spectral and temporal shapes of the ICS and SR emissions: while the early unabsorbed SR contribution has a spectral energy density $F_\nu \propto \nu^{-0.6}$, ICS has $F_\nu \propto e^{-E/E_p(t)}$ and satisfies the $E t^2$ law.

In order to test whether the prompt X-ray peak around 1000 s and the UVOT peaks between 30 and 50 ks belong to the same ICS pulse, we have plotted in Fig. 9c the energy fluxes between 5 ks and 150 ks measured with the UVOT filters, de-reddened for Galactic extinction [$E(B - V) = 0.14$, Campana et al. (2006b)] and scaled by the $E t^2$ law, together with the unabsorbed energy flux in the 0.3 -10 keV band of the prompt X-ray pulse which was measured with the XRT (Campana et al. 2006b). Each de-reddened energy flux in the UVOT filters at time t was converted to energy flux density using the UVOT energy band widths, $\Delta E = h \nu \Delta \lambda / \lambda^2$, with $\Delta \lambda = 75, 98, 88, 70, 51$ and 76 nm the FWHM of the V, B,

U, UVW1, UVM1 and UVW2 filters of the Swift UVOT, with central wavelengths, $\lambda = 544$ nm, 439 nm, 345 nm, 251 nm, 217 nm, and 188 nm respectively. These energy flux densities were multiplied by the XRT band width and plotted at time $(\nu/\nu_x)^{0.5} t$, where $h\nu_x = 5.15$ keV is the central energy of the 0.3 -10 keV band. As can be seen from Fig. 9d, the XRT and UVOT data near their peak times satisfy the $E t^2$ (or $\sqrt{\nu} t$) law quite well. The very large differences between peak times and peak energy fluxes in the Swift *XUVO* bands simply disappear in the scaled-time plot, and the peaks' shapes coincide.

In Tables 3,4 and Figs. 10a,b we further test the $E t^2$ law for the peak-energy flux (PEF) and peak-time in the different UVOT filters. Though these results are flawless, there remain the small deviations from the $E t^2$ law in Fig. 9d, which may be due to its approximate nature, our rough spectral integrations, a non-negligible contribution from the SN at a relatively early time and/or a significant SR contribution to the UVOT light curves. There is a strong indication for the latter possibility: the spectrum obtained from the de-reddened UVOT data at $t < 5$ ks is consistent either with the $E t^2$ law (Fig. 9d) or with a SR spectrum below the frequency bend, $F_\nu \propto \nu^{-0.6}$. This is demonstrated in Fig. 9c, where we have plotted the UVOT de-reddened data of Campana et al. (2006b) in the form $\nu^{0.6} F_\nu(t)$, which, for $t \ll (a, t_{exp})$ and $\beta = 0.6$ in Eq. (34), should be proportional to $t^{0.4}$. The line in the figure shows that it is. A black-body shape, $F_\nu \propto \nu^2$, multiplied by $\nu^{0.6}$ would have, for instance, separated the *V* and *UVW2* bands by a factor ~ 14 , entirely inconsistent with Fig. 9c.

From the above relatively model-independent analysis we have concluded that the *UVO* light curves observed prior to the dominance of the associated SN, and the early-time X-ray data, are consistent with ICS of glory light by a jet of CBs breaking out from SN2006aj, while they are inconsistent with a black-body radiation from a shock break-out from the stellar envelope of the progenitor star. But, can the detailed broad-band observations of this XRF be reproduced by the CB model in greater detail?

Amati et al. (2006) showed that XRF 060218 complies with the so-called ‘Amati correlation’ (Amati 2002) for GRBs and XRFs and concluded that this implies that XRF 060218 *was not* a GRB viewed far off axis. In the CB model the conclusion of the same argument is the opposite one. The observed correlation between peak and isotropic energies of GRBs *and* XRFs is a prediction (Dar & De Rújula 2000, DD2004, Dado, Dar & De Rújula 2007b) trivially following from the kinematics of ICS. The fact that XRF 060218 complies with it corroborates that it *was* a GRB viewed far off axis. In this model, the isotropic equivalent γ -ray energy emission of a typical CB is $\approx 0.8 \times 10^{44} [\delta_0]^3$ erg (DD2004). Thus, the reported $E_{iso} \approx (6.2 \pm 0.3) \times 10^{49}$ erg implies that the CB which generated the dominant peak of XRF 060218 had $\delta_0 \sim 92$. It then follows from Eq. (6) that its measured $E_p = 4.6$ keV implies (for the typical $kT(0) \sim 1$ eV) a Lorentz factor $\gamma_0 \sim 103$, $\gamma_0 \theta \approx 1.1$ and a viewing angle

$\theta \sim 1.08 \times 10^{-2}$ rad, an order of magnitude larger than the typical GRB value $\theta \sim 1$ mrad.

The best-sampled data set of XRF 060218 is the XRT 0.3 -10 keV light curve (Campana et al. 2006b). Thus, we fit these data first, with prompt ICS emission plus SR. We assume that the prompt ICS emission is dominated by two pulses: an early one preceding the main pulse, as suggested by the hardness ratio and the BAT light curve. The SR contribution was calculated using Eqs. (22,26) for a constant-density ISM, with the previously-derived $\gamma_0 \theta = 1.1$, the standard $\beta_X = 1.1$, and a best-fit value for t_b . The result is Fig. 10c; the corresponding Swift-XRT hardness ratio is shown in Fig. 10d (DDD2008a), and the AG parameters are listed in Table 1. Next, we use the $E t^2$ law for ICS to predict the UVOT and BAT light curves. The results are Fig. 10e for the de-reddened UVOT light curve in the UVW2 filter, and Fig. 10f for the BAT light curve in the 15-150 keV band.

We conclude that the XRF 060218/SN2006aj pair is in full agreement with the predictions of the CB model. The rich structure of its *UVO* AG is as expected. Its X-ray light curve has the canonical GRB shape (stretched in time) and consistent with the observed E_p and E_{iso} . All of these results are explicitly dependent on the fact that XRFs are GRBs produced by CBs with smaller Doppler factors, because they are viewed at larger angles or have smaller Lorentz factors. The data on this XRF are inconsistent with a black-body component generated by a shock break-out through the stellar envelope, or by any other mechanism. The start time of the X-ray emission does not constrain the exact time of the core’s collapse before the launch of the CBs, nor the possible ejection of other CBs farther off axis, prior⁶ to the trigger-time of XRF 060218.

6. Conclusions and outlook

The rich data on GRBs gathered after the launch of Swift, as interpreted in the CB model and as we have discussed here and in recent papers (e.g. Dado et al. 2006, 2007, 2008a, 2008b) has taught us several things:

- Two radiation mechanisms, inverse Compton scattering and synchrotron radiation, suffice within the CB model to provide a very simple and accurate description of long-duration GRBs and XRFs and their afterglows. Simple as they are, these two mechanisms and the bursts’ environments generate the rich structure and variety of the light curves at all frequencies and times.

⁶Intriguingly, Swift detected γ rays from the same direction over a month earlier on January 17, 2006 (Barbier, et al. 2006).

- The historical distinction between prompt and afterglow phases is replaced by a physical distinction: the relative dominance of the Compton or synchrotron mechanisms at different, frequency-dependent times.
- The relatively narrow pulses of the γ -ray signal, the somewhat wider prompt flares of X-rays, and the much wider humps sometimes seen at *UVOIR* frequencies in XRFs, have a common origin. They are generated by inverse Compton scattering.
- The synchrotron radiation component dominates the prompt optical emission in ordinary GRBs, the broad-band afterglow in GRBs and XRFs and the late-time flares of both types of events.
- The early-time XRT and UVOT data on XRF 060218 are inconsistent with a black-body emission from a shock break-out through the stellar envelope. Instead, they support the CB-model interpretation of ICS of glory light by an early jet of CBs from what is later seen as SN2006aj. The start time of the X-ray emission does not constrain the exact time of the core’s collapse before the launch of the CBs, nor the possible ejection of other CBs farther off axis.
- Despite its simplicity and approximate nature, the CB model continues to provide an extremely successful description of long GRBs and XRFs. Its testable predictions, so far, are in complete agreement with the main established properties of their prompt emission and of the afterglow at all times and frequencies.

We re-emphasize that the results presented in this paper are based on direct applications of our previously published explicit predictions. Our master formulae, Eq. (12) for ICS and Eqs. (22, 26, 33) for the synchrotron component describe all the data very well. But, could they just be very lucky guesses? The general properties of the data are predictions. But, when fitting cases with many flares, are we not ‘over-parametrizing’ the results? Finally, the $E t^2$ law plays an important role. Could it also be trivially derived in a different theory?

When their collimated radiation points to the observer, GRBs are the brightest sources in the sky. In the context of the CB model and of the simplicity of its underlying physics, GRBs are not persistent mysteries, nor ‘the biggest of explosions after the Big Bang’, nor a constant source of surprises, exceptions and new requirements. Instead, they are well-understood and can be used as cosmological tools, to study the history of the intergalactic medium and of star formation up to large redshifts, and to locate SN explosions at a very early stage. As interpreted in the CB model, GRBs are not ‘standard candles’, their use in ‘Hubble-like’ analyses would require further elaboration. The GRB conundra have been

reduced to just one: ‘how does a SN manage to sprout mighty jets?’ The increasingly well-studied ejecta of quasars and microquasars, no doubt also fired in catastrophic accretion episodes on compact central objects, provides observational hints with which, so far, theory and simulations cannot compete.

The CB model underlies a unified theory of high energy astrophysical phenomena. The information gathered in our study of GRBs can be used to understand, also in very simple terms, other phenomena. The most notable is (non-solar) cosmic rays. We allege (Dar et al. 1992, Dar & Plaga 1999) that they are simply the charged ISM particles scattered by CBs, in complete analogy with the ICS of light by the same CBs. This results in a successful description of the spectra of all primary cosmic-ray nuclei and electrons at all observed energies (Dar and De Rújula 2006a). The CB model also predicts very simply the spectrum of the gamma background radiation and explains its directional properties (Dar & De Rújula 2001a, 2006b). Other phenomena understood in simple terms include the properties of cooling core clusters (Colafrancesco, Dar & De Rújula 2003) and of intergalactic magnetic fields (Dar & De Rújula 2005). The model may even have a say in ‘astrobiology’ (Dar, Laor & Shaviv 1998, Dar & De Rújula 2001b).

Acknowledgment: A.D. would like to thank the Theory Division of CERN for its hospitality during this work. We would also like to thank S. Campana, G. Cusumano, P. Ferrero, D. Grupe, D. A. Kann, K. L. Page and S. Vaughan, for making available to us the tabulated data of their published X-ray and optical light curves of Swift GRBs and an anonymous referee for an exceptionally constructive and useful report.

REFERENCES

- Akerlof, C., et al. 1999, *Nature*, 398, 400
- Amati, L., et al. 1999, *NuPhS*, 69, 656
- Amati, L., Frontera, F., Tavani, M., et al. 2002, *A&A*, 390, 81
- Amati, L., 2006, *MNRAS*, 372, 233
- Band, D., et al. 1993, *ApJ*, 413, 281
- Barbier, L., et al. 2006, *GCN Circ* 4780
- Beckmann, V. et al. 2008, *GCN Circ* 7450
- Berger, E. & Gladders, M. 2006, *GCN* 5170
- Berger, E., et al. 2005, *ApJ*, 634, 501
- Bloom, J. S., Frail, D. A. & Kulkarni, S. R. 2003, *ApJ*, 594, 674
- Bloom, J. S. et al. 2008, *arXiv:0803.3215*
- Blustin, A. J. 2007, *Phil. Trans. Royal. Soc. A*, 365, 1263
- Burrows, D. N. & Racusin, J. 2007, *astro-ph/0702633*
- Butler, R. 2007, *ApJ*, 656, 1001
- Campana, S., et al. 2006a, *GCN* 5162
- Campana, S., et al. 2006b, *Nature*, 442, 1008
- Cenko, S. B., et al. 2006, *ApJ*, 652, 490
- Coburn, W. & Boggs, S. E. 2003, *Nature*, 423, 415
- Colafrancesco, S., Dar, A. & De Rújula, A. 2004, *A&A*, 413, 441
- Colgate, S. A. 1968, *CaJPS*, 46, 476
- Covino, S., et al. 2006, *Il Nuovo Cimento B*, 121, 1171
- Covino, S., et al. 2008, *MNRAS*, 388, 347
- Cucchiara, A. et al. 2008, *GCN Circ.* 7456

- Curran, P. A., et al. 2006, arXiv: astro-ph/0610067
- Cusumano, G., et al. 2006a, ApJ, 639, 316
- Cusumano, G., et al. 2006b, GCN 4775
- Cwiok, M. et al. 2008, GCN Circ. 7445
- Dado, S. & Dar, A. 2005, Nuovo Cimento 120, 731
- Dado, S. & Dar, A. 2008, ApJ, in press (arXiv:0807.1962)
- Dado, S., Dar, A. & De Rújula, A. 2002a, A&A, 388, 1079 (DDD2002a)
- Dado, S., Dar, A. & De Rújula, A. 2003a, A&A, 401, 243 (DDD2003a)
- Dado, S., Dar, A. & De Rújula, A. 2003b, ApJ, 593, 961 (DDD2003b)
- Dado, S., Dar, A. & De Rújula, A. 2003c, ApJ, 594, L89 (DDD2003a)
- Dado, S., Dar, A. & De Rújula, A. 2004, A&A, 422, 381 (DDD2004)
- Dado, S., Dar, A. & De Rújula, A. 2006, ApJ, 646, L21 (DDD2006)
- Dado, S., Dar, A. & De Rújula, A. 2007a, ApJ, 663, 400 (DDD2007a)
- Dado, S., Dar, A. & De Rújula, A. 2007b, arXiv: astro-ph/0701294 (DDD2007b)
- Dado, S., Dar, A. & De Rújula, A. 2007c, arXiv: arXiv:0706.0880
- Dado, S., Dar, A. & De Rújula, A. 2008a, ApJ, 681, 1408 (DDD2008a)
- Dado, S., Dar, A. & De Rújula, A. 2008b, ApJ, 680, 517 (DDD2008b)
- Dai, X., et al. 2007, ApJ, 658, 509
- Dai, X., et al. 2008, ApJ, 682L, 77
- Dar, A. 1998, ApJ, 500, L93
- Dar, A. 2005, arXiv:arXiv: astro-ph/0405386
- Dar, A. 2006, ChJAS, 6, 301
- Dar, A. & Plaga, R. 1999, A&A, 349, 259
- Dar, A. & De Rújula, A. 2000a, arXiv: astro-ph/0008474

- Dar, A. & De Rújula, A. 2000b, arXiv: astro-ph/0012227
- Dar, A. & De Rújula, A. 2001a, MNRAS, 323, 391
- Dar, A. & De Rújula, A. 2001b, *Astrophysics and Gamma Ray Physics in Space* (eds. A. Morselli and P. Picozza), Frascati Physics Series Vol. XXIV pp. 513-523 (arXiv: astro-ph/0110162)
- Dar, A. & De Rújula, A. 2004, Physics Reports, 405, 203 (DD2004)
- Dar, A. & De Rújula, A. 2005, PRD, 72, 123002
- Dar, A. & De Rújula, A. 2008, Physics Reports, 466, 179
- Dar, A., Laor, A. & Shaviv, N. J. 1998, PRL, 80, 5813
- Dar, A. & Plaga, R. 1999, A&A, 349, 259
- Della Valle, M., et al. 2006, Nature 444, 1050
- De Rújula, A. 1987, Phys. Lett. 193, 514
- De Rújula, A. 2007a , arXiv:0707.0283
- De Rújula, A. 2007b, arXiv:0711.0970 (in press)
- De Rújula, A. 2008, arXiv:0801.0397
- Evans, P. A., et al. 2007, A&A, 469, 379
- Fenimore, E. E., et al. 1995, ApJ, 448, L101
- Ferrero, P., et al. 2006, A&A, 457, 857
- Ferrero, P. et al. 2008, arXiv:0804.2457
- Frederiksen, J. T. et al. 2003, arXiv: astro-ph/0303360
- Frederiksen, J.T., et al. 2004, Astrophys. J. 608, L13
- French, J., & Jelinek, M. 2006, GCN 5165
- Frail, D. A., et al. 2001, ApJ, 562, L55
- Galama, T. J. et al. 1998a, ApJ, 497, L13
- Galama, T. J. et al. 1998b, Nature, 395, 670

- Gal-Yam, A., et al. 2006, *Nature*, 444, 1053
- Ghisellini, G., Celotti, A., & Lazzati, D. 2000, *MNRAS*, 316, L5
- Gomboc, A., et al. 2008, *ApJ*, 687, 443
- Golenetskii, S. et al. 2008, *GCN Circ.* 7482
- Guenther, E. W., et al. 2006, *GCN* 4863
- Hao, H., et al. 2007, *ApJ*, 659, 99,
- Heise, J., et al. 2001, *Gamma-Ray Bursts in the Afterglow Era*, (Eds. E. Costa, F. Frontera, and J. Hjorth) Springer-Verlag, p. 16
- Hjorth, J., et al. 2003, *Nature*, 423, 847
- Huang, K. Y., et al. 2007, *ApJ*, 654, L25
- Jakobsson, P., et al. 2006, *A&A*, 460, L13
- Kalemci, E., et al. 2007, *ApJS*, 169, 75
- Karpov, S. et al. 2008, *GCN Circ.* 7558
- Khamitov, I. M., et al. 2007, *AstL*, 33, 797
- Kocevski, D., Ryde, F. & Liang, E. 2003, *ApJ*, 596, 389
- Kocevski, D., et al. 2007, *ApJ*, 663, 1180.
- Krimm, H., et al. 2005, *GCN Circ.* 3117
- Kumar, P., et al. 2007, *MNRAS*, 376, L57
- Li, W., et al. 2003, *ApJ*, 586, L9
- Liang E. W., et al. 2007, *ApJ*, 653, L81
- Liang, E. W., et al. 2008, *ApJ*, 675, L528
- Lipkin, Y. M., et al. 2004, *ApJ*, 606, 381
- Malesani, D. et al. 2004, *ApJ*, 609, L5
- Malesani, D., et al. 2008, *arXiv:0805.1188*

- Mangano, V., et al. 2007, *A&A*, 470, 105
- Marshall, F., et al. 2006, *GCN Circ.* 4779
- Masetti, N., et al. 2006, *GCN Circ.* 4803
- Mazzali, P. A., et al. 2006, *ApJ*, 645, 1323
- McGlynn, S., et al. 2007, *A&A*, 466, 895
- Mészáros, P. 2002, *ARA&A*, 40, 137
- Mészáros, P. 2006, *Rept. Prog. Phys.* 69, 2259
- Mirabal, L. & Halpern, J. P., 2006, *GCN* 4709
- Mirabal, L., et al. 2006, *ApJ*, 643, L99
- Mirabel, I.F. & Rodriguez, L.F. 1999 *ARA&A*, 37, 409.
- Modjaz, M., et al. 2008, *arXiv:0805.2201*
- Molinari, E., et al. 2007, *A&A*, 469, L13
- Monfardini, A., et al. 2006, *ApJ*, 648, 1125
- Nisenson, P. & Papaliolios, C. 2001, *ApJ*, 548, L201
- Nishikawa, K.-I. et al. 2003, *ApJ*, 595, 555
- Nousek, J., et al. 2006, *ApJ*, 642, 389
- Nysewander, M., et al. 2007, *arXiv:0708.3444*
- O’Brien, P. T., et al. 2006, *ApJ*, 647, 1213
- Page, K. L. et al. 2007, *ApJ*, 663, 1125
- Panaitescu, A., et al. 2006, *MNRAS*, 369, 2059
- Panaitescu, A. 2007, *MNRAS*, 380, 374
- Parsons, A., et al. 2006, *GCN* 5370
- Perley, D. A., et al. 2008, *ApJ*, 672, 449
- Pian, E., et al. 2006, *Nature*, 442, 1011

- Piran, T. 1999, *Physics Reports*, 314, 575
- Piran, T. 2000, *Physics Reports*, 333, 529
- Piran, T. 2005, *RMP*, 76, 1143
- Piro, L., et al. 1998, *A&A*, 331, L41
- Piro, L., et al. 2000, *Science*, 290, 955
- Quimby, R. M., et al. 2006, *ApJ*, 640, 402
- Quimby, R. M., et al. 2006b, *GCN Circ.* 5366
- Racusin, J. L. et al. 2008a, *arXiv:0801.4749*
- Racusin, J. L. et al. 2008b, *GCN Circ.* 7427
- Racusin, J. L. et al. 2008, *GCN Circ.* 7459
- Reeves, J. N., et al. 2002, *Nature*, 416, 512
- Rhoads, J. E. 1997, *ApJ*, 487, L1
- Rhoads, J. E. 1999, *ApJ*, 525, 737
- Rodriguez, L.F. & Mirabel, I.F. 1998, *New Astron. Rev.* 42, 649.
- Romano, P., et al. 2006, *A&A* 450, 59
- Rykoff, E. S., et al. 2004, 2004, *ApJ*, 601, 1013
- Salamanca, I. et al. 1998, *MNRAS*, 300, L17S
- Salamanca, I., Terlevich, R. J. & Tenorio-Tagle, G. 2002, *MNRAS*, 330, 844
- Sari, R., Piran, T. & Halpern, J. P. 1999, *ApJ*, 519, L17
- Sato, G., et al. 2007, *ApJ* 657, 359
- Schady, P., et al. 2007, *MNRAS*, 380, 1041
- Schaefer, B. E. 2007, *ApJ*, 663, 1125
- Shaviv, N. J. & Dar, A. 1995, *ApJ*, 447, 863
- Sollerman et al. 2006, *A&A*, 454, 503

- Soderberg, A. M., et al. 2006, *Nature*, 442, 1014
- Soderberg, A. M., et al. 2008, *Nature*, 453, 469
- Stanek, K. Z., et al. 2003, *ApJ*, 591, L17
- Stanek, K. Z., et al. 2007, *ApJ*, 654 L21
- Thöne, C. C., et al. 2006, *GCN* 5373
- Thöne, C. C., et al. 2008a, *A&A*, 489, 37
- Thöne, C. C., et al. 2008b, *arXiv:0806.1182*
- Turatto, M., et al. 2000, *ApJ*, 534, L57
- Vaughan, S., et al. 2006, *ApJ*, 638, 920
- Vestrand, J. A. et al. 2006, *Nature*, 442, 172.
- Vreeswijk, P. M. et al. 2008, *GCN Circ.* 7444
- Yonetoku, D., et al. 2004, *ApJ*. 609, 935
- Watson, D., et al. 2003, *ApJ*, 595, L29
- Waxman, E. 2003a, *Lect. Notes Phys.* 598, 393
- Waxman, E., Meszaros, P. & Campana, S. 2007, *ApJ*, 667, 351
- Wiersema, K., et al. 2007, *A&A*, 464, 529.
- Wigger, C., et al. 2004, *ApJ*, 613, 1088
- Wigger, C., et al. 2008, *ApJ*, 675, 553
- Willis, D. R., et al. 2005, *A&A*, 439, 245
- Wozniak, P. R., et al. 2005, *ApJ*, 627, L13
- Wozniak, P. R., et al. 2006, *ApJ*, 642, L99
- Wozniak, P., et al. 2008, *GCN Circ.* 7464
- Yoshida, A., et al. 1999, *A&AS*, 138, 433
- Yoshida, A., et al. 2001, *ApJ*, 557, L27

Wu, B. & Fenimore, E. 2000, ApJ, 535, L29

Zhang, B. & Mészáros, P. 2004, IJMPA, 19, 2385

Zhang, B. 2007, ChjAA, 7, 1

Zhang, B-B., Liang, E-W. & Zhang, B. 2007, ApJ, 666, 1002

Ziaeeppour, H., et al. 2008, MNRAS, 385, 453

Table 1. CB-model afterglow parameters.

GRB/XRF	t_0 [s]	$\theta \gamma_0$	p
060729	(606)	(2.52)	2.20
061121	248	1.42	2.20
050315	12362	0.965	2.20
061007	40	$\ll 1$	2.20
061126	142	1.08	1.84
080319B	72	($\ll 1$)	2.16
060211A	64596	0.54	2.11
061110A	29402	0.81	2.04
080307	28893	1.00	2.13
051021B	13092	0.82	2.24
080303	15196	0.79	2.15
070220	1314	0.64	2.16
060526	1840	0.93	2.20
060206	2570	1.035	2.20
050820A	2692	1.128	2.22
060418	< 60	1.73	2.20
071010A	857	1.21	1.92
050318	273	1.61	2.19
050326	379	1.28	2.16
051008	1233	1.17	2.20
050814	7737	1.14	2.18
061019	194	2.22	2.20
070306	1437	1.91	2.20
060813	273	1.60	2.20
070521	551	1.33	2.23
080207	95	0.98	1.87
060807	9867	1.02	2.21
070419B	1146	0.99	2.20
070420	60	2.00	2.22
050319	73	0.92	2.20
050319	999	2.05	2.22

Table 1—Continued

GRB/XRF	t_0 [s]	$\theta \gamma_0$	p
060605	(< 1000)	(1.00)	2.20
060607A	(54)	(1.07)	2.20
060218	267	1.10	1.94

Table 2. Time parameters in Eq. (12) for the two last prompt X-ray flares.

GRB/XRF	Band	t_1 [s]	Δt_1 [s]	t_2 [s]	Δt_2 [s]
060729	X	122	6.2	153	19.1 s
061121	X	52	12.4	97	18.8
050315	X	-5	6.9	16.4	5.4
061007	X	23	5.5		
061126	X	4.4	7.8		
080319	X	37	5.0		
060211A	X	79	30		
061110A	X	35	54		
080307	X	0	373		
051021B	X	0	67		
080303	X	0	114		
070220	X	0	75		
060526	X	233	16.4	272	31.6
060206	X	581	43.2	4187	549
050820A	X	205	29	2173	2225
060418	X	60	12	118	9.8
071010A	X	18990	30968		
050814	X			0	2074
070306	X	154	20	364	50
060813	X	37	58	0	246
070521	X	0	222		
060807	X	0	26		4635
070419B	X	106	41	134	87
070420	X	0	54		
050319	X	0	54	2003	
060605	X	0	83	67	154
060607A	X				
060218	X	0	950		

Table 3. Peak energy flux (PEF) and peak flux density (PFD) of XRF 060218 in the Swift UVOT filters, corrected for Galactic reddening $E(B - V) = 0.14$; and the PFD predicted, using the $E t^2$ law, from the XRT unabsorbed PEF in the 0.3 -10 keV band.

Filter	λ [nm]	E(center) [eV]	FWHM	PEF [erg cm ⁻² s ⁻¹]	PFD [μ Jansky]	Predicted PFD [μ Jansky]
UVW2	188	6.60	76 nm	$(2.29 \pm 0.23) \times 10^{-12}$	355 ± 36	374 ± 135
UVM1	217	5.71	51 nm	$(1.30 \pm 0.10) \times 10^{-12}$	399 ± 31	374 ± 135
UVW1	251	4.94	70 nm	$(1.17 \pm 0.12) \times 10^{-12}$	352 ± 37	374 ± 135
<i>U</i>	345	3.55	88 nm	$(8.89 \pm 0.85) \times 10^{-13}$	406 ± 44	374 ± 135
<i>B</i>	439	2.83	98 nm	$(5.99 \pm 0.56) \times 10^{-13}$	393 ± 37	374 ± 135
<i>V</i>	544	2.28	75 nm	$(2.59 \pm 0.10) \times 10^{-13}$	340 ± 34	374 ± 135

Table 4. Peak times of the energy flux of XRF 060218 in the Swift XRT and UVOT filters and their expected values from the $E t^2$ law.

Band	E(eff) [eV]	Observed t_{peak} [s]	CB Model t_{peak} [s]
X	5150	985 ± 50	985 ± 50 (input)
X	3000	$1,310 \pm 90$	$1,290 \pm 65$
X	600	$2,790 \pm 2,550$	$2,770 \pm 150$
UVW2	6.60	$25,800 \pm 5,000$	$27,500 \pm 1,400$
UVM1	5.71	$36,208 \pm 8,000$	$29,600 \pm 1,800$
UVW1	4.94	$41,984 \pm 10,000$	$32,000 \pm 1,600$
<i>U</i>	3.59	$42,864 \pm 10,000$	$37,500 \pm 1,900$
<i>B</i>	2.82	$39,600 \pm 15,000$	$42,000 \pm 2,100$
<i>V</i>	2.28	$47,776 \pm 10,000$	$47,000 \pm 2,400$

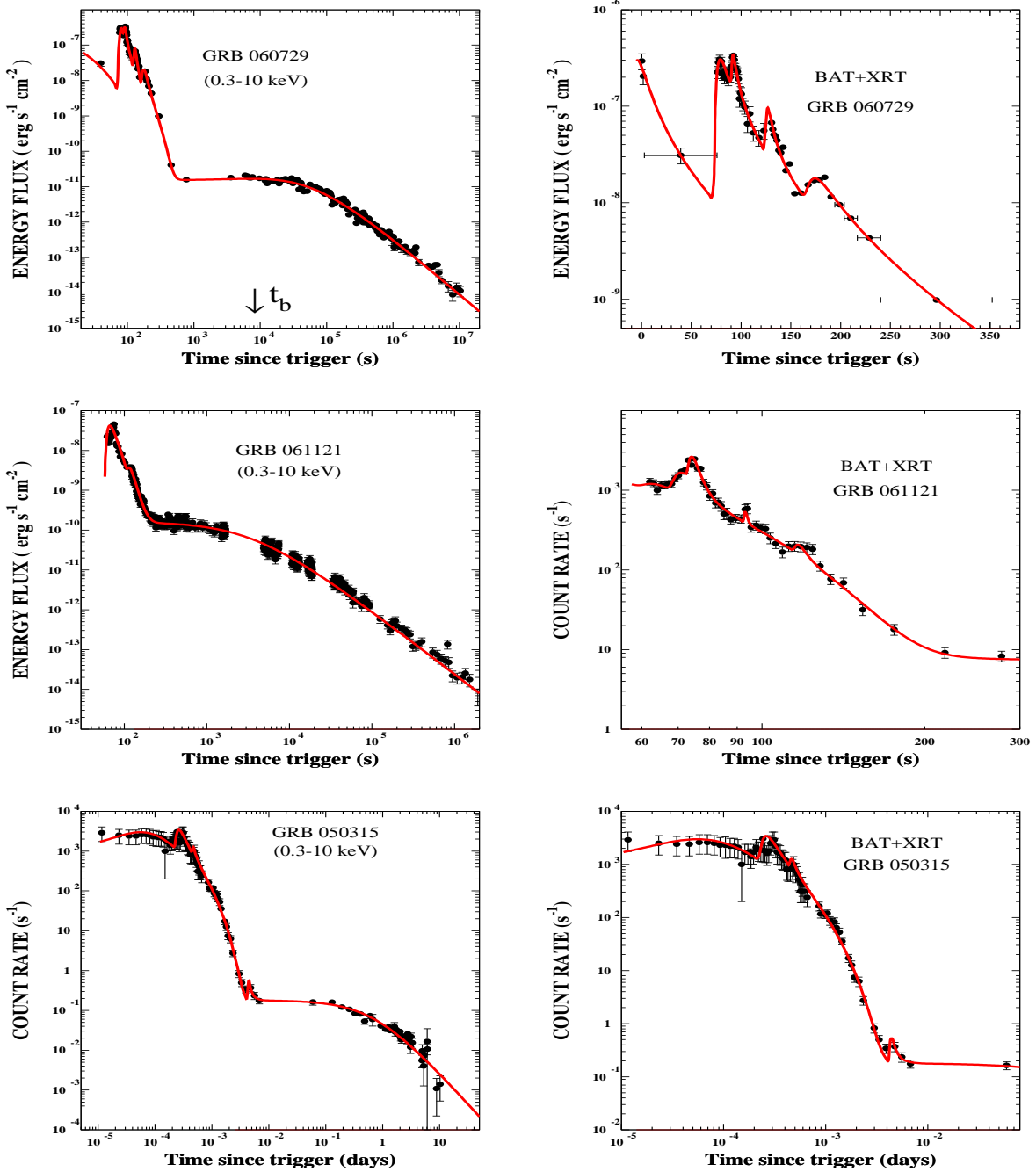


Fig. 1.— Comparison between Swift observations of canonical GRB X-ray light curves and their CB-model description for: **Top left (a):** GRB 060729. **Top right (b):** GRB 060729 at early time. **Middle left (c):** GRB 061121. **Middle right (d):** GRB 061121 at early time. **Bottom left (e):** GRB 050319. **Bottom right (f):** GRB 050319 at early time.

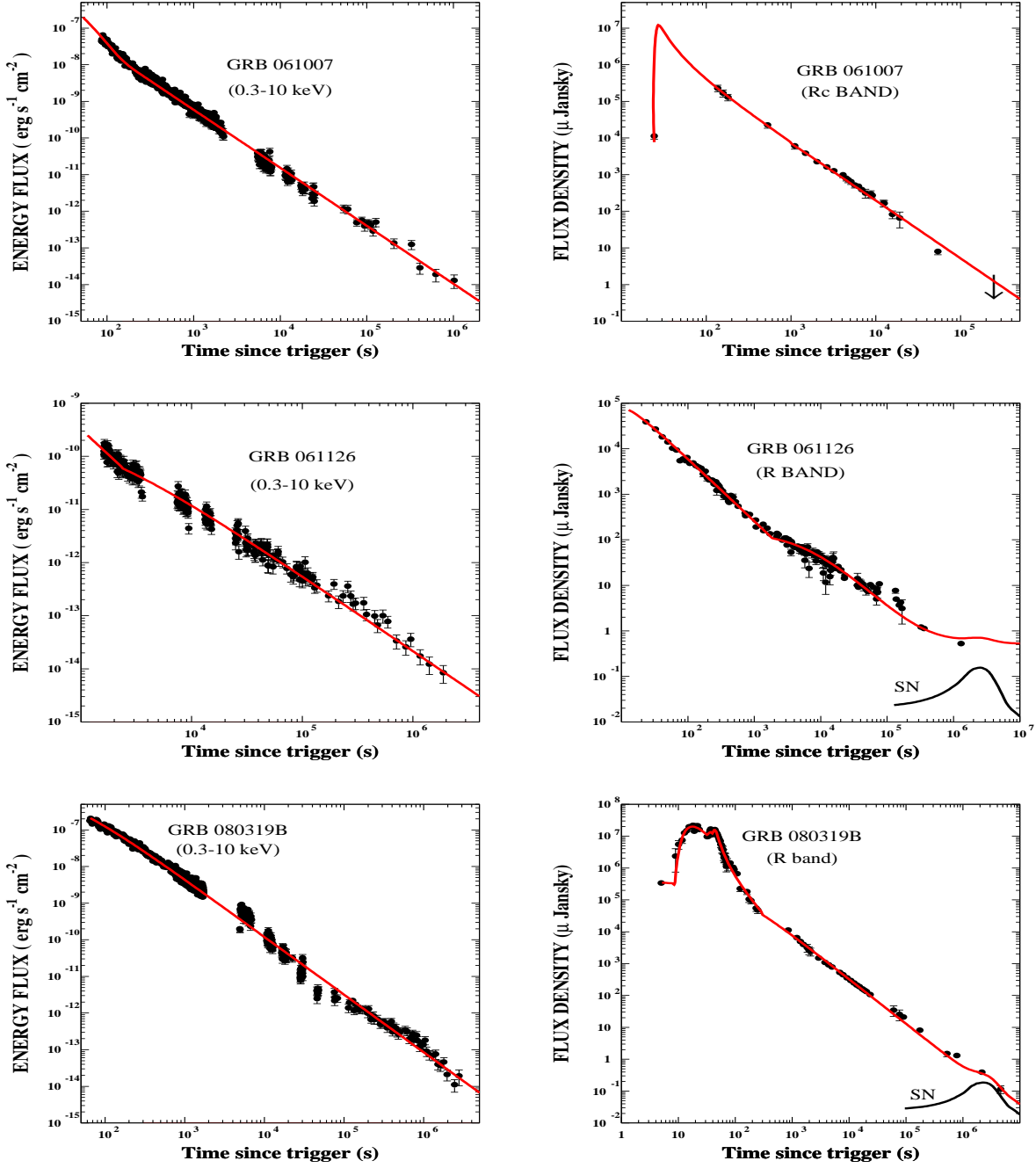


Fig. 2.— Comparison between broad-band observations of GRBs with single-power-law decaying AGs and their CB-model description, for: **Top left (a):** The X-ray light curve of GRB 061007. **Top right (b):** The *R*-band light curve of GRB 061007. **Middle left (c):** The X-ray light curve of GRB 061126. **Middle right (d):** The *R*-band light curve of GRB 061126. **Bottom left (e):** The X-ray light curve of GRB 080319B. **Bottom right (f):** The *R*-band light curve of GRB 080319B. Some SN1998bw-like SN contributions are shown.

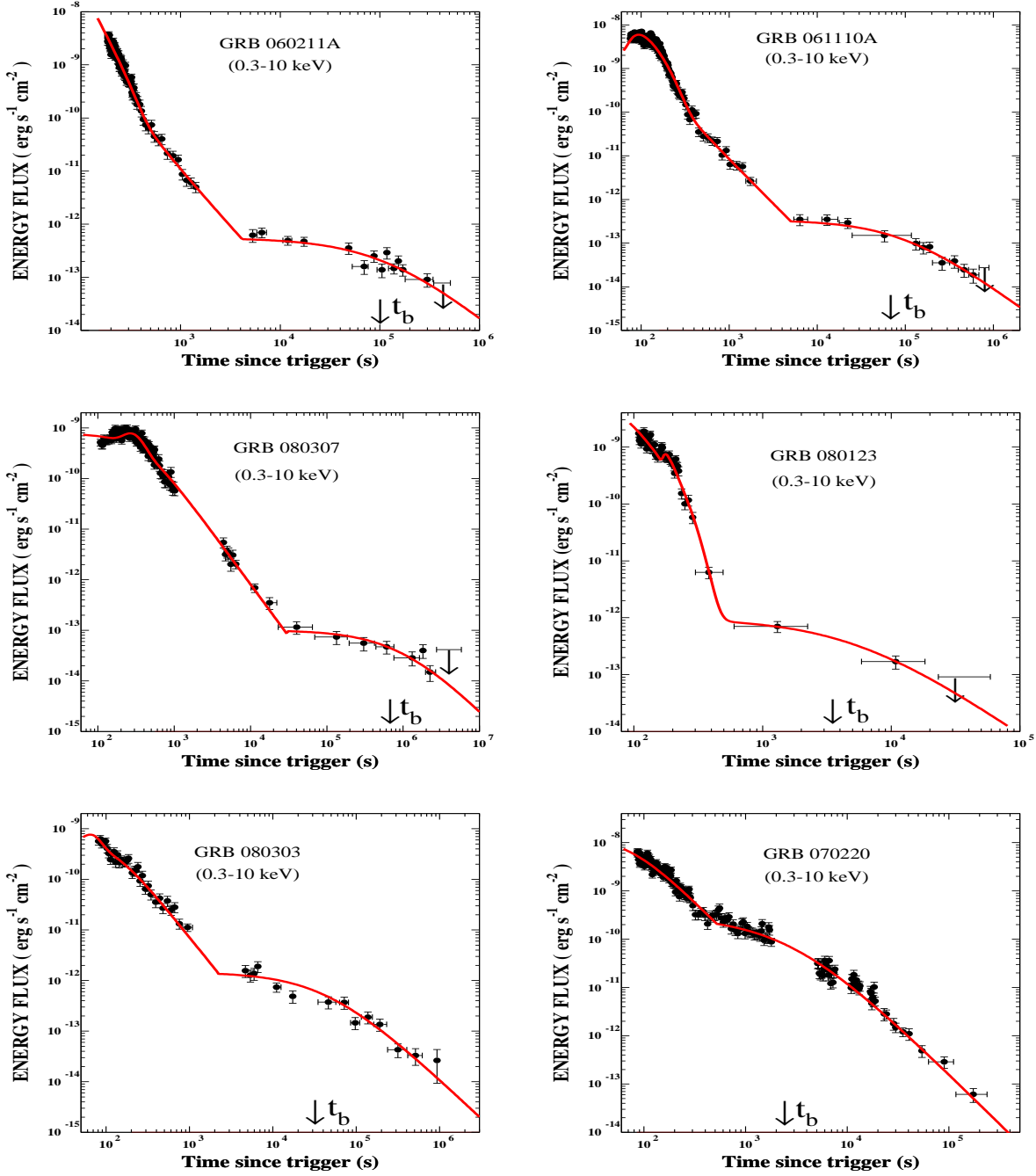


Fig. 3.— Comparison between ‘semi-canonical’ X-ray light curves of Swift GRBs and their CB-model description for: **Top left (a):** GRB 060211A. **Top right (b):** GRB 061110A. **Middle left (c):** GRB 080307. **Middle right (d):** GRB 051021B. **Bottom left (e):** GRB 080303. **Bottom right (f):** GRB 070220.

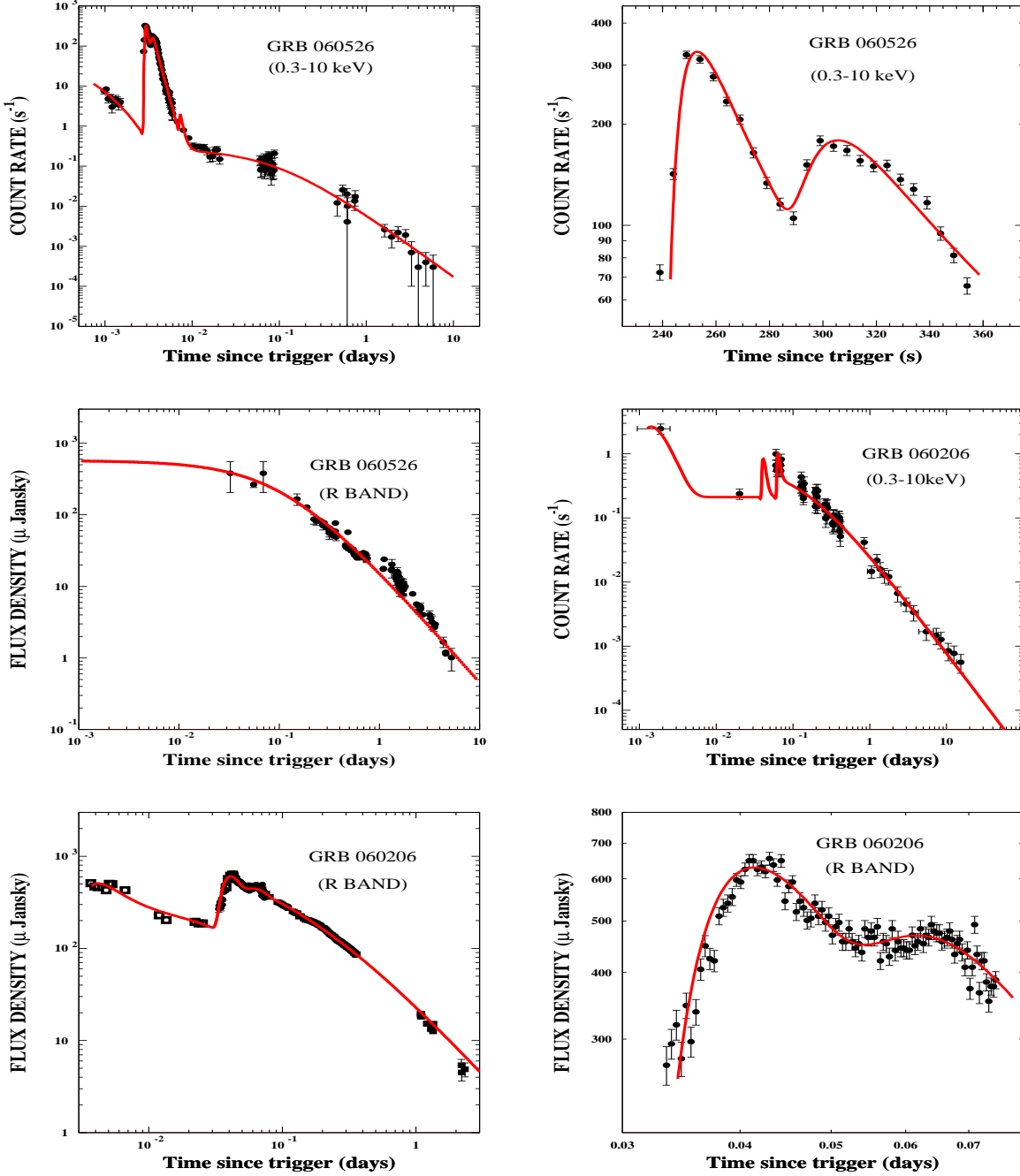


Fig. 4.— Comparison between broad-band observations of GRBs with chromatic early-time afterglow and their CB-model descriptions for: **Top left (a):** The XRT light curve of GRB 060526. **Top right (b):** The early X-ray ICS flares of GRB 060526. **Middle left (c):** The *R*-band light curve of GRB 060526. **Middle right (d):** The XRT light curve of GRB 060206. **Bottom left (e):** The *R*-band light curve of GRB 060206. **Bottom right (f):** Enlarged view of two-early time *R*-band SR flares and their CB-model description.

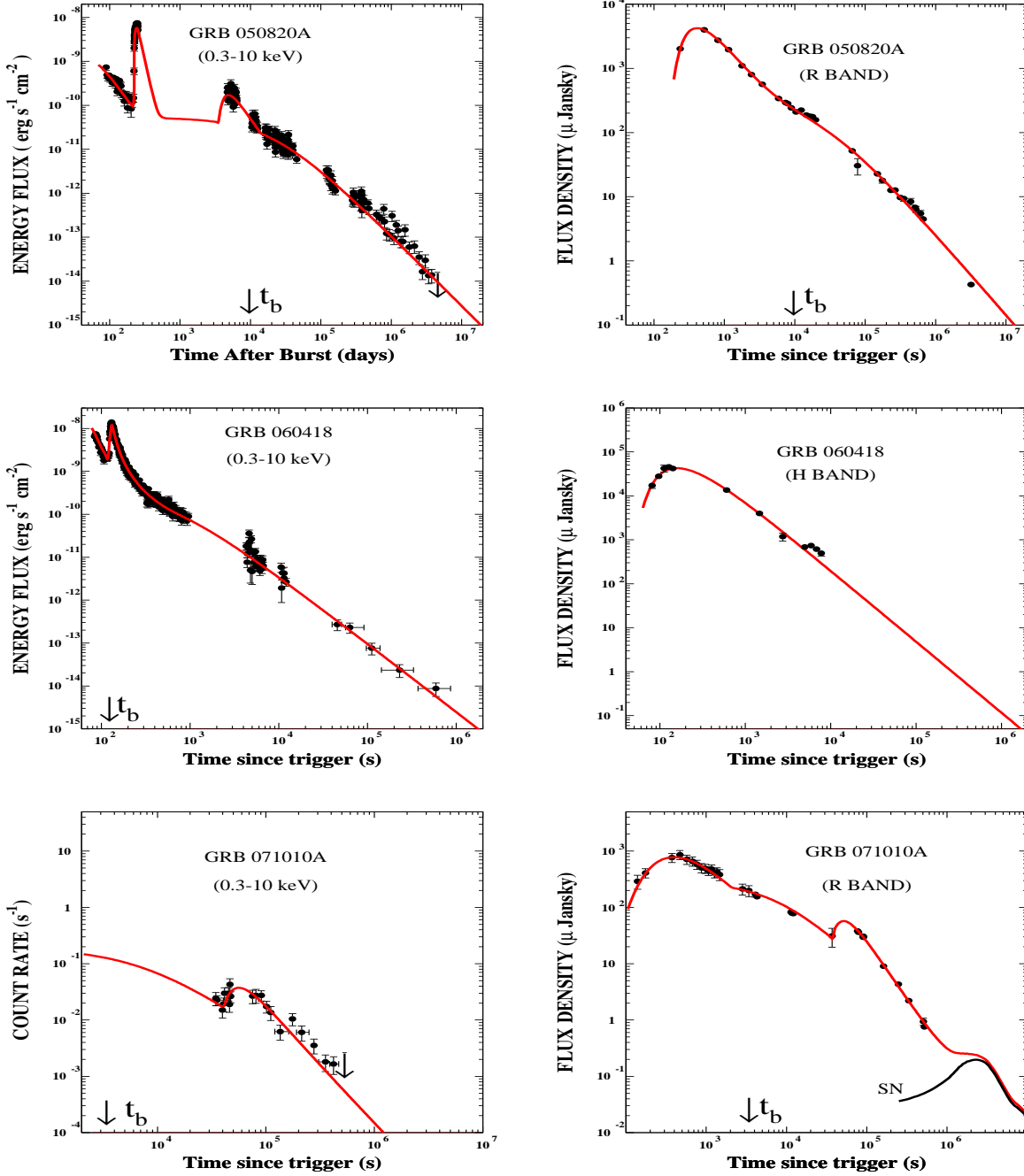


Fig. 5.— Comparison between broad-band observations of GRBs with chromatic early-time afterglow and their CB-model descriptions for: **Top left (a)**: The X-ray light curve of GRB 050820A. **Top right (b)**: The *R*-band light curve of GRB 050820A. **Middle left (c)**: The X-ray light curve of GRB 060418. **Middle right (d)**: The *H*-band light curve of GRB 060418. **Bottom left (e)**: The X-ray light curve of GRB 071010A. **Bottom right (f)**: The *R*-band light curve of GRB 071010A.

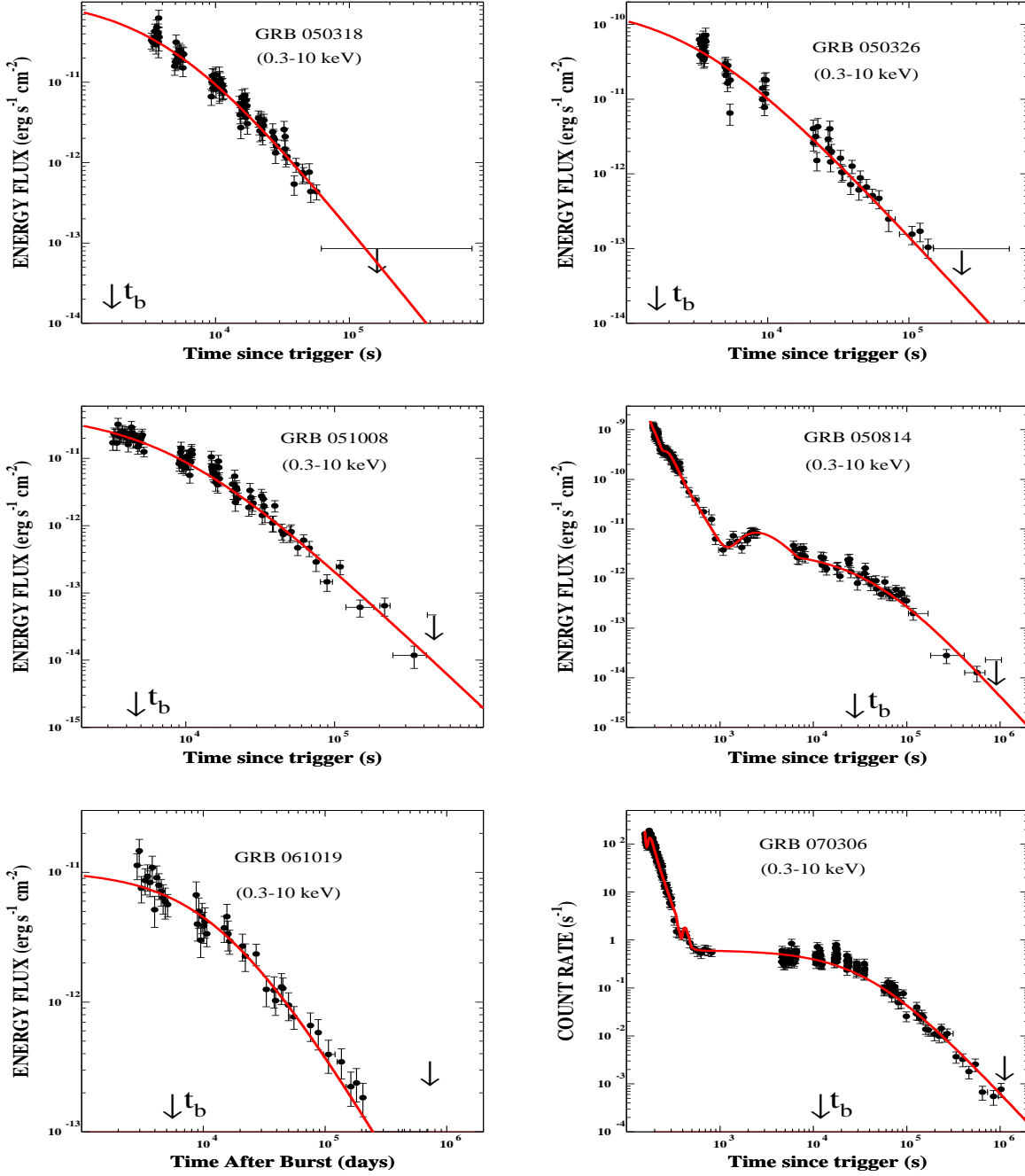


Fig. 6.— Comparison between XRT-light curves of Swift GRBs (Evans et al. 2007) with late time decay index $\alpha > 2$ and their CB-model descriptions assuming an isothermal-sphere density profile, for: **Top left (a):** GRB 050318. **Top right (b):** GRB 050326. **Middle left (c):** GRB 051008. **Middle right (d):** GRB 050814. **Bottom left (e):** GRB 061019. **Bottom right (f):** GRB 070306.

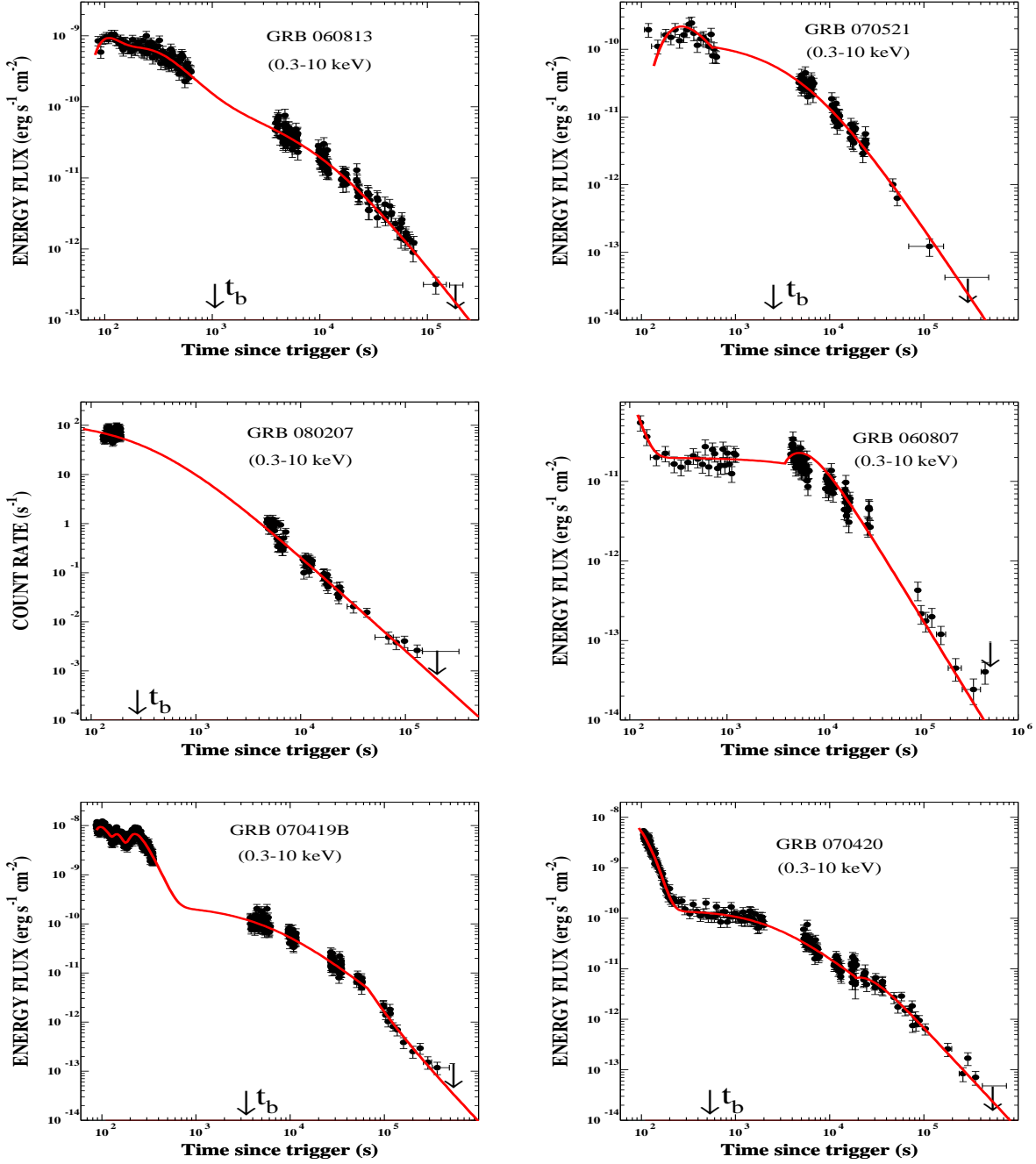


Fig. 7.— Comparison between the Swift XRT-light curves with late-time decay index ($\alpha > 2$) or a late-time flare and their CB-model description for: **Top left (a)**: GRB 060813, with a step decay. **Top right (b)**: GRB 070521, with a step decay. **Middle left (c)**: GRB 080207, with a step decay. **Middle right (d)**: GRB 060807, with a flare. **Bottom left (e)**: GRB 070419B, with a flare. **Bottom right (f)**: GRB 070420, with a flare.

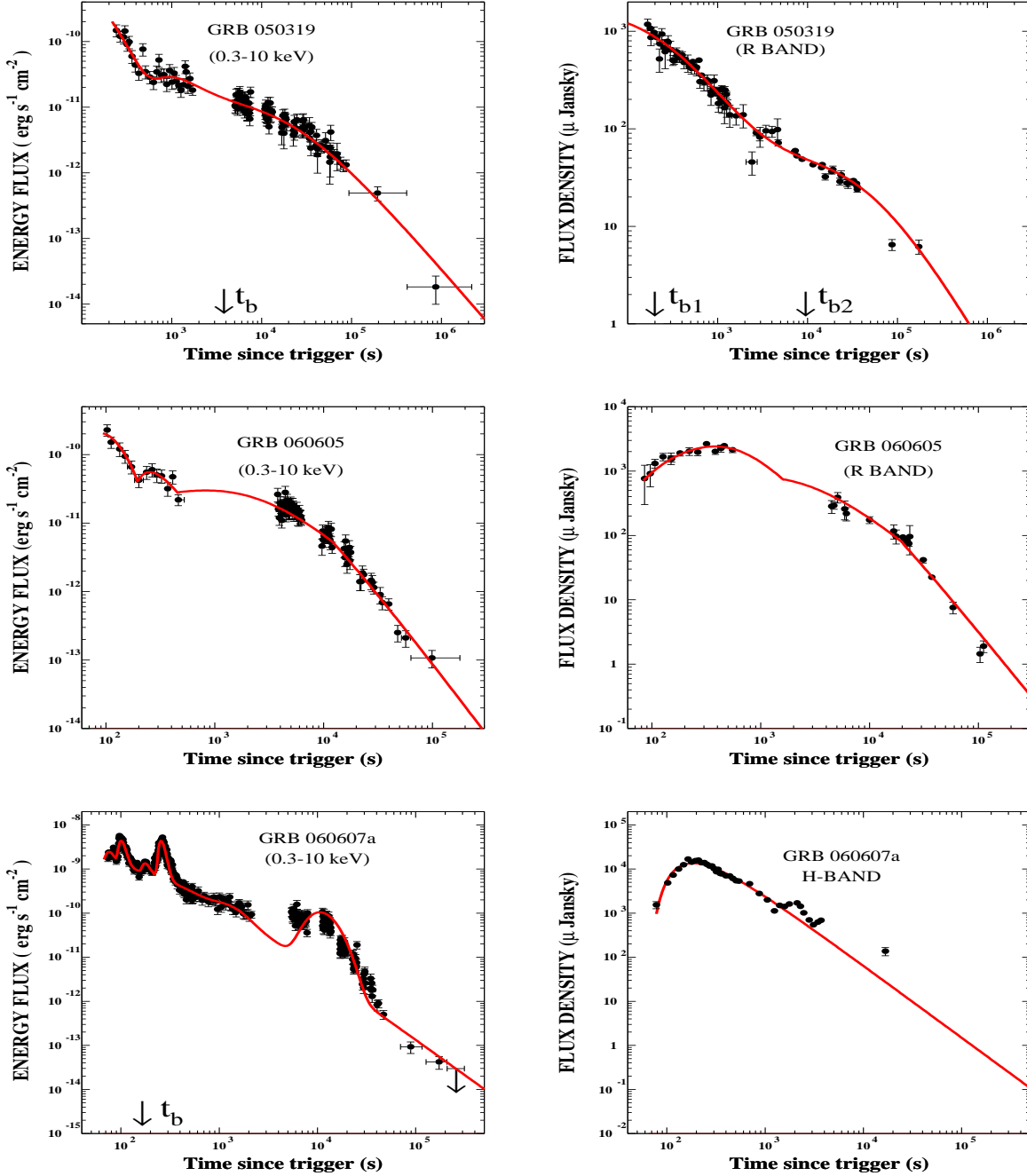


Fig. 8.— Comparison between complex chromatic light curves of GRBs and their CB-model description for: **Top left (a):** The X-ray light curve of GRB 050319. **Top right (b):** The R -band light curve of GRB 050319. **Middle left (c):** The X-ray light curve of GRB 060605. **Middle right (d):** The R_c -band light curve of GRB 060605. **Bottom left (e):** The X-ray light curve of GRB 060607A. **Bottom right (f):** The H -band light curve of GRB 060607.

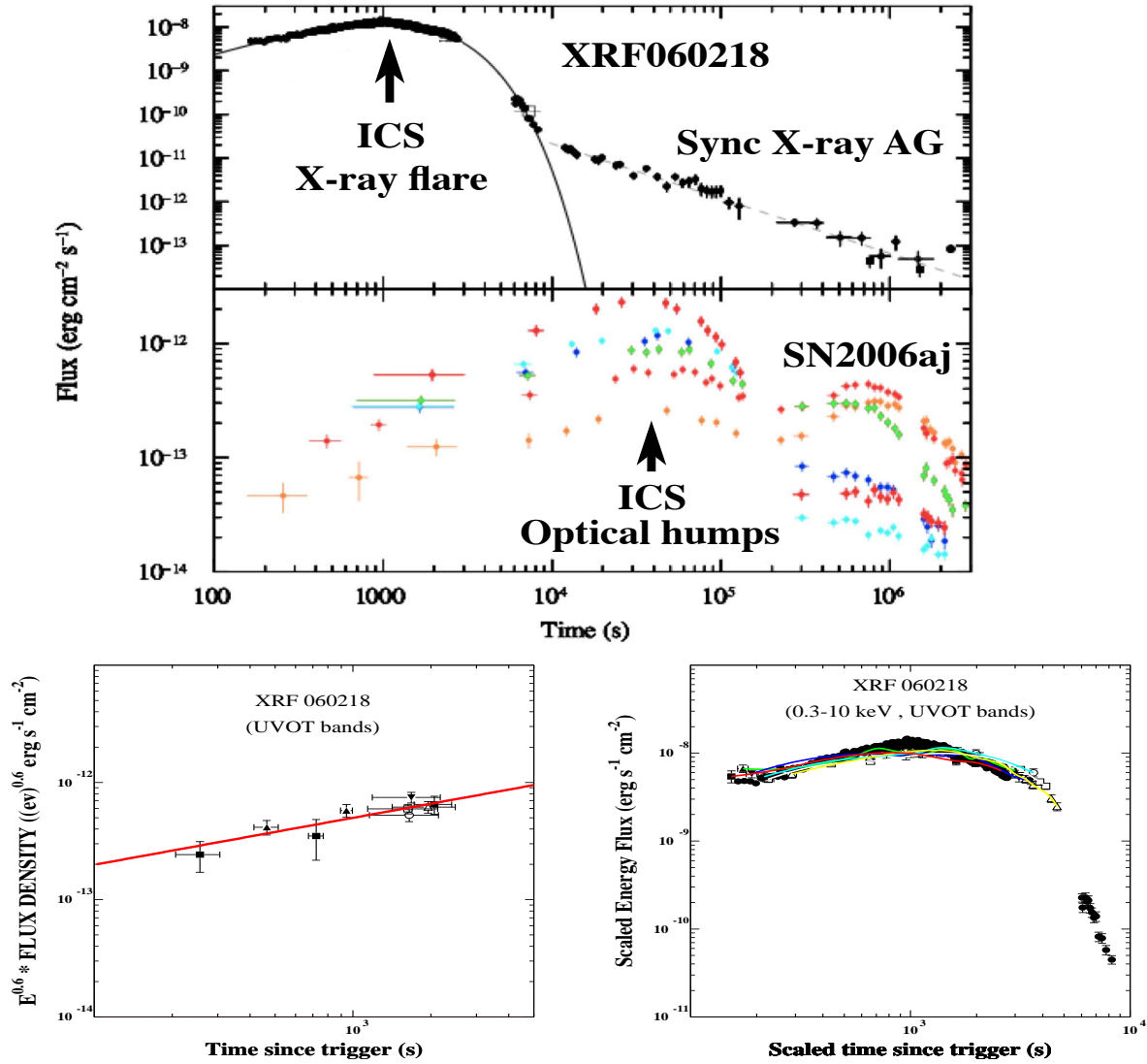


Fig. 9.— X-ray and *UVO* light curves of XRF 060218/SN2006aj. (a) and (b): **The top figure** (Campana et al. 2006b). Upper half (a): The unabsorbed 0.3–10 keV Swift-XRT light curve. The line is a sum of a cut-off power-law and a black body with fitted time-dependent radius and temperature. The dashed line is their best-fit power law for $t > 10$ ks. The arrows indicate rough peak-flux times. Lower half (b): Energy fluxes corrected for reddening: red: *V*; green: *B*; blue: *U*, light blue: UVW1; magenta: UVM1 and yellow: UVW2. **Bottom left (c)**: De-reddened energy flux densities multiplied by $\nu^{0.6}$, predicted to have the slope of the plotted line ($\propto t^{0.4}$). **Bottom right (d)**: The unabsorbed and the de-reddened energy fluxes, divided by the band-width ratios, plotted as functions of $(E/E_X)^{1/2} t$.

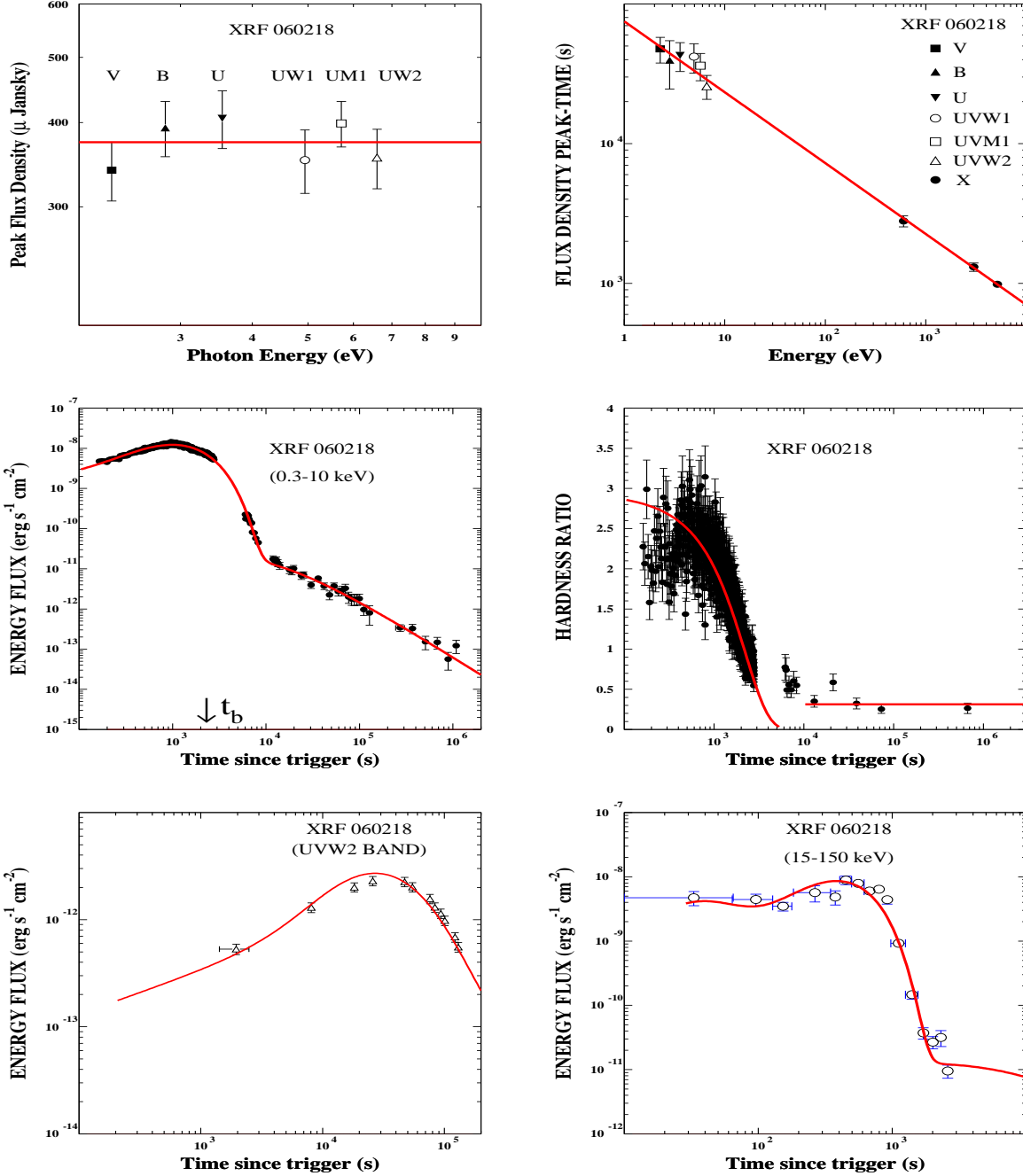


Fig. 10.— XRF 060218: data and CB-model predictions. **Top left (a):** De-reddened UVOT PEF divided by $E \Delta\lambda/\lambda$, plotted at the central energy of each band. The line is the prediction of the $E t^2$ law. **Top right (b):** PEF times in XRT and UVOT filters, and the $E t^2$ law (red line’s slope). **Middle left (c):** Swift unabsorbed XRT light curve. The ICS \rightarrow SR transition is at ~ 9 ks. **Middle right (d):** XRT hardness ratio. **Bottom left (e):** UVW2 light curve. **Bottom Right (f):** BAT 30-150 keV γ -ray light curve and its expected shape from the $E t^2$ law. An early peak, hinted by the hardness ratio, was added.